Master of Science Thesis

Design of residual-based unresolved-scale models using time-averaged solution data.

Luis Carlos Navarro Hernández

December 4, 2015

Faculty of Aerospace Engineering

Delft University of Technology

Design of residual-based unresolved-scale models using time-averaged solution data.

Master of Science Thesis

For obtaining the degree of Master of Science in Aerospace Engineering
at Delft University of Technology

Luis Carlos Navarro Hernández

December 4, 2015

Faculty of Aerospace Engineering · Delft University of Technology

Delft University of Technology

DELFT UNIVERSITY OF TECHNOLOGY
DEPARTMENT OF AERODYNAMICS

The undersigned hereby certify that they have read and recommend to the Faculty of Aerospace Engineering for acceptance the thesis entitled **"Design of residual-based unresolved-scale models using time-averaged solution data."** by **Luis Carlos Navarro Hernández** in fulfillment of the requirements for the degree of **Master of Science**.

Dated: December 4, 2015

Supervisors:

____
Dr. Steven J. Hulshoff

____
Prof.dr. Stefan Hickel

____
Dr. Marios Kotsonis

____
Dr.ir. Axelle Viré

Acknowledgments

I would like to express the gratitude I feel towards the endless support that I have received throughout the pursue of my master's degree. First an foremost, my parents and brother have been an unlimited source of motivation and support, not only during this stage of my life, but in any project I have chosen to pursue. The example set by my hard working parents has always been and will always be an inspiration to keep going further.

I also want to thank my thesis supervisor Dr. Steven J. Hulshoff, whose expertise and passion for the topics we explored is also a source of inspiration for me. His continuous support proved invaluable for the completion of this project and I thank all the effort he dedicated to my project.

Finally, I would like to thank the Mexican National Council of Science and Technology (CONACyT), for sponsoring my studies at TU-Delft, given that completing this master's is something which would have not been possible without this aid.

Table of Contents

List of Figures

List of Tables

Chapter 1

Introduction

The phenomenon of turbulent flow is rarely absent from most cases of relevance for aerospace engineering. It is normally characterized by complex three-dimensional, time dependent events which influence the overall behavior of a flow in far from trivial ways. The capabilities of modern computers have made accurate approximations of PDE-governed physical problems cost and time effective. In particular, turbulent flow can be described by the Navier-Stokes equations (NSE). Nevertheless, currently available resources come very short of the ones required for a full computation of all the flow structures involved in turbulence.

Resolving every turbulent structure in the flow is known as Direct Numerical Solution (DNS). Today this is a viable answer for flows of low Reynolds numbers. However, the Re of aerospace engineering relevance are commonly orders of magnitude above those of DNS feasible cases, presenting interactions in space and time between sub-millimetre and meters-long scales. Cost inhibits the use of smallest-scale capturing grids, and creates the need for alternate approaches, capable of approximating the effects of these smallest scales without truly solving for them.

Among the most popular methods for modelling such structures, are Reynolds Averaged Navier-Stokes (RANS) computations, and Large-Eddy Simulation (LES). Both of these employ a separation of the quantities in the NSE. While the former splits them into mean and fluctuating components, the latter performs a filtering operation (normally involving the scale size as a parameter), thus obtaining large (resolved) and small (unresolved) scales [Pope (2000)]. These separations however introduce what is known as a closure problem in the new forms of the NSE. Additional equations are now required; normally referred to as turbulence models, for RANS, and Sub-grid Scale (SGS) models for LES. Many of these models have been developed over decades.

Even though these methods provide feasible alternatives for turbulence computation, their scenario-dependent accuracy and viability makes them suitable only for specific circumstances or applications. Specifically, while RANS requires relatively low computational effort, its statistical nature renders it unfit for calculating regions with large fluctuations, such as massively separated flows. On the other hand, the grid requirements for an accurate computation of high Reynolds near-wall flows using LES, generate costs which scale similarly to those of DNS (a quasi-DNS) [Nikitin et al. (2000)]. More often than not, a single case will present a mixture of regions which no individual method can fully cover. The currently available solution to this difficulty is to use a Hybrid method.

Hybrid methods

The attempt at tackling the individual shortcomings of both methods was proposed by Spalart et al. (1997) in a formulation known as Detached Eddy Simulation (DES). In it, the most energetic scales away from the walls are solved by LES, while the energy dissipating structures close to the walls are modeled by an inexpensive RANS method. While in theory this approach poses a simple solution, and being this the essential idea behind most modern Hybrid methods, the reality is that this coupling is far from trivial, leading to consistency issues stemming from the arbitrary nature of this combination.

A DES approach focuses only on solving turbulent fluctuations away from the walls, while performing the boundary layer (BL) calculations through statistical methods. As Menter et al. (2012) point out, this approach can be set apart from other hybrids in the sense that it computes the complete boundary layer in a RANS mode. On the other hand, more recent methods employ RANS for the innermost part of the BL, switching to LES as soon as the characteristic lengths allow for it. Such methods have come to be called Wall-modelled LES (WMLES). Finally, in some cases we are concerned with turbulent structures only in specific regions of an otherwise stable flow; for which a RANS computation of the majority of the domain can be made, employing LES only in the regions of expected instabilities. What is known as an embedded LES is obtained in this manner. Whichever is the situation, there is still a question concerning the actual coupling methods, for which two major categories can be established. The methods themselves commonly present complex formulations and procedures, which impedes placing them in either category unambiguously. Based Froehlich and von Terzi (2008), a quick overview is provided now.

Segregated modeling. Also known as zonal approach in other literature; the segregated approach performs nearly independent LES and RANS calculations in the different zones. The methods are coupled by transferring information between the zones, in the form of boundary conditions, which makes the solved quantities (such as pressure or velocities) no longer continuous at the interface. For this to be a truly hybrid method, such interfaces must allow a bidirectional transfer of information.

Unified modeling. Also known as blended, global or non-zonal approaches; these make use of the structural similarity between the filtered LES equations and the RANS. Generalizing the momentum equation for both methods, we obtain:

$$\rho\frac{\partial\overline{u_i}}{\partial t}+\rho\frac{\partial\overline{u_i}\;\overline{u_j}}{\partial x_j}=-\frac{\partial\overline{p}}{\partial x_i}+\mu\frac{\partial^2\overline{u_i}}{\partial {x_j}^2}+\frac{\partial}{\partial x_j}\tau_{ij}^{model}$$

Where the τ_{ij}^{model} represents the stress tensor as described by the particular method and turbulence model. The focus of unified modelling is to create a τ_{ij}^{model} as a function of a RANS and an LES turbulence models. A combination of the form:

$$\tau_{ij}^{model}=f^{LES}\tau_{ij}^{LES}+f^{RANS}\tau_{ij}^{RANS}$$

can be made, where f^{LES} and f^{RANS} are local blending coefficients and functions of the particular approach parameters. If such coefficients become binary, an absolute local switch of models is achieved with a clear boundary between the LES and RANS regions, which is called an interfaced approach. Yet, this boundary can still adapt according to the solution state, for which a soft interface is said to exist. The one which remains static throughout time is consequently called a hard interface.

However, when employing the turbulence model as a methods switch, as pointed out by Xiao and Jenny (2012), a fundamental inconsistency is introduced, granted that the structural similarity in the transport equations does not account for the composition of the τ terms. While the solution separation in LES is done by (normally spatial) filtering, RANS employs statistical methods i.e. quantity averaging. Even though many SGS models for LES are based on turbulence models for RANS [Froehlich and von Terzi (2008)], in blending the models the inconsistency manifests as non-physical behaviors in the flow.

General issues

The most important problem is observed when at the interface, the model switching takes place. The eddy viscosity (EV) of the RANS model is reduced while the turbulent structures on the LES side have not yet developed, given the relatively steady boundary conditions originating from the RANS region. Since the turbulent fluctuations in the resolved side develop relatively slowly, not enough turbulent stress is generated to compensate for the previously mentioned reduction in EV. The end result of these events is what is known as a log-law shift, or Log-Layer Mismatch (LLM). Initial attempts to attack these issues have been pursued by Baggett (1998); Hamba (2002); Piomelli et al. (2002). These have a variety of approaches, including changes in the velocity gradients, methods order inversion, grid refinements, and interface-wall proximity alterations. The conclusion, however, is that there is a level of resilience in the LLM [Piomelli et al. (2003); Larsson et al. (2007)].

A number of solutions to this problem have been proposed since. These span a variety of approaches, making a precise classification difficult. However, in a general sense, they can be separated into three categories i.e. model blending functions, stochastic forcing and consistent approaches. Model blending functions combat the LLM issue by modifying the equations which mix the turbulence models. In an attempt to achieve a smoother transition, and allow the models appropriate eddy development lengths in the Scale-Resolving Simulation (SRS) mode [Menter and Egorov (2010)], some researchers have introduced formulations that range from length scale redefinitions, to adaptive blending functions. Regarding stochastic forcing, artificially exciting the fluctuations at the interfaces has proven to be an effective solution to the LLM. This can be achieved either by the introduction of stochastic functions, or by mapping pre-computed databases. Furthermore, the former variant of the technique can be categorized in the nature of the forcing functions (random signals, Fourier modes, etc.), while the latter can introduce databases from different methods (LES or DNS mainly). While the previously mentioned approaches try to solve the LLM issue through an improvement of the coupling conditions, a dynamic adaptation of the models, or ad hoc introduction of turbulence-triggering-fluctuations, none addresses the root cause; which relies in the fundamentally inconsistent coupling of the transport equations or regions.

A recent solution attacking the issue at its core is proposed by Xiao and Jenny (2012). A basic difference with respect to other methods, is that both RANS and LES are employed simultaneously in the entire domain, rather than on localized regions. The LES is computed in a mesh which does not allow recovering a QDNS solution in the near-wall, meaning that the boundary layer is not properly modeled and even less properly solved in its small-scale region. However, the LES structure-capturing capabilities are exploited in the core flow, where the turbulent fluctuations present characteristic lengths which go in accordance with the grid spacing, and thus with the computational capabilities. In a different, yet overlapping mesh, a RANS solution is obtained, which at first glance might seem redundant, given that portions of it will be "discarded and replaced" by the results of the LES. The near-wall region in this grid receives special attention regarding the "y refinement", to properly capture the wall behavior under the statistical frame of a RANS method. The clear observation then is that both methods employ their own optimized grids. Once this is made, the essential proposition of this method comes in place. The momentum equations are now "coupled" through an additional force term called the Drift Term, instead of through the turbulence/SGS model.

Scope of this thesis

With these concepts in mind, the aim of this research is to propose a consistent hybrid framework based on a Variational Multiscale Method (VMM) formulation of the NSE for turbulence computation; where a residual-based algebraic expression for an SGS model will be employed as a coupling term. While, the final solution will be obtained under an LES scheme, the SGS model will contain information drawn from reference data from an overlapping domain as in Xiao and Jenny (2012). Since the VMM results in an SGS model which depends on the large-scale residual, the coupling will effectively vanish within sufficiently resolved regions without the need of additional controlling terms. The expected result is therefore to demonstrate that reference-data-enriched LES is possible with a solid understanding of the behavior of the proposed SGS models as a basis for future work. Such work might be the use of Goal-Oriented optimization or Artificial Neural Network techniques to adjust the SGS model and thus reproduce the statistics of RANS. This work will investigate the potential of such methods by considering the design of residual based SGS models with locally adjustable behavior and determining their ability to influence the statistics of the flow.

The objectives to achieve this aim, and thus the structure of this thesis can be stated as follows: As a proof of concept, the scheme will initially be constructed for the simulation of nonlinear dynamics in a unidimensional domain under the Burgers equation (BE). The relatively low computational cost of solving this problem will allow to verify that the formulation has been appropriately posed, as well as initially investigating the effects of manipulating the stabilization parameters. After obtaining initial results and an understanding of the behavior of the formulation, a similar set-up is proposed for the VMM version of the NSE. The test case in this three-dimensional context is the channel flow. Although in a broad sense, the adaptation from BE to NSE will involve a notoriously more complex mathematical formulation, the essential ideas remain unmodified.

Chapter 2

The Variational Multiscale Method applied to the Burgers equation

Traditional LES relies on a filtering operator for scale separation. Even though in concept this filter can hav an arbitrary length scale, in practice the grid size is normally employed to determine which turbulent scales are to be resolved, and which are to be modeled. A rather different framework based on the Variational Multiscale Method (VMM) was proposed for LES by Hughes et al. (2000), for which scale separation is invoked ab initio. Initial VMM approaches to account for the effects of the unresolved scales in the flow were oriented to EV models given the accumulated experience with them. Later VMM developed SGS models using approximations of their dynamic equations. The latter will be considered here. This chapter will present this methodology in the context of the Burgers equation along with initial tests to demonstrate its applicability. The concepts and derivations introduced here will set the base framework for this work.

2.1 The Burgers equation

Formulated by the Dutch scientist Jan Martinus Burgers and introduced in Burgers (1948), the nonlinear advection-diffusion equation can be regarded as a simplification of the NSE. It results from the neglection of the pressure term, and is today more commonly known as the Burgers equation. An analytic method of solution was developed by Burgers (1954) based on a Hopf-Cole transformation, and has wave-like solutions. However, its real relevance to the field of aerodynamics is that "it contains essential ingredients of turbulent flow" [Nieuwstadt and Steketee (2012)]. It possesses a forward energy cascade deriving from its nonlinear term, and high dissipation in regions of high gradients, where its viscous term becomes large.

While in essence, this equation retains important features of real turbulent flow behavior, it still lacks a crucial characteristic, which is its chaotic response to variations in the initial conditions. Given this, its application regarding the understanding of the SGS models and their behavior is limited but nonetheless useful. This equation and its relevance to this research will be exposed in the remainder of this chapter.

2.1.1 The problem in strong form

Let Ω be an open, connected, bounded subset of $\mathbb{R}^d$, with boundary Γ, and in which, for the Burgers equation, $d = 1$, representing a spatial domain $[0, X]$ [Hughes et al. (2000, 2004)]. A space-time domain Q for a time interval $]0, T[$ in Ω is given by $Q = \Omega \times]0, T[$. In this domain, for the space and time variables $0 \leq x \leq X$, and $0 \leq t \leq T$ respectively, the strong form of the Burgers equation is given by:

$$\frac{\partial u}{\partial t} + u\frac{\partial u}{\partial x} = \nu\frac{\partial^2 u}{\partial x^2} + f(x,t) \tag{2.1}$$

Or in simplified notation, with the derivatives expressed as subindices:

$$u_t + uu_x - \nu u_{xx} = f(x,t) \tag{2.2}$$

Where $\nu = 1/Re$ stands for the (positive and constant) kinematic viscosity, and f represents a body force (per unit length) vector. Introducing the **Burgers differential operator**:

$$\mathcal{L} = \frac{\partial}{\partial t} + u\frac{\partial}{\partial x} - \nu\frac{\partial^2}{\partial x^2} \tag{2.3}$$

The problem can finally be expressed as:

Find $u : Q \mapsto \mathbb{R}$ such that:

$$\mathcal{L}u = f(x,t) \quad \text{in } \Omega \tag{2.4}$$
$$u = g(x,t) \quad \text{on } \Gamma \tag{2.5}$$

2.1.2 The problem in weak form

Now let us consider the trial solution and testing function spaces:

$$u \in \quad \mathcal{S} \subset H^1(\Omega) \tag{2.6}$$
$$w \in \quad \mathcal{V} \subset H^1(\Omega) \tag{2.7}$$

Where H^1 represents a Sobolev space of square integrable functions given by:

$$H^1 = \{h | h \in L^2, h_x \in L^2\} \tag{2.8}$$
$$L^2 = \{h | \int_\Omega (h)^2 d\Omega < \infty\} \tag{2.9}$$

Following a standard Galerkin method, the strong form of the Burgers equation (2.1) is multiplied by the test function w and integrated over the (spatial) domain yielding:

$$\int_{\Omega} w(u_t + uu_x - \nu u_{xx} - f)dx = 0 \tag{2.10}$$

Which when employing a standard bilinear form notation $(\cdot,\cdot)_\Omega$ for the $L_2(\Omega)$ inner product, and the Burgers differential operator (2.3); can now expressed in compact notation as:

$$(w, \mathcal{L}u)_\Omega = (w, f)_\Omega \tag{2.11}$$

After integration by parts, the form:

$$(w, u_t)_\Omega + w\frac{u^2}{2}\bigg|_\Omega - \left(w_x, \frac{u^2}{2}\right)_\Omega - w\nu u_x\bigg|_\Omega + (w_x, \nu u_x)_\Omega = (w, f)_\Omega \tag{2.12}$$

is obtained, which when assuming $\mathcal{S}$ and $\mathcal{V}$ fulfill:

$$u = g \quad \text{on } \Gamma \quad \forall u \in \mathcal{S} \tag{2.13}$$
$$w = 0 \quad \text{on } \Gamma \quad \forall w \in \mathcal{V} \tag{2.14}$$

and for simplicity purposes, henceforth omitting the Ω subindex in the standard bilinear form notation; becomes:

$$(w, u_t) - \left(w_x, \frac{u^2}{2}\right) + (w_x, \nu u_x) = (w, f) \tag{2.15}$$

It is now possible to define the **weak Burgers operator** as:

$$B(w, u) = (w, u_t) - \left(w_x, \frac{u^2}{2}\right) + (w_x, \nu u_x) \tag{2.16}$$

With which the weak form of the problem finally reads as:

Find $u \in \mathcal{S} \quad \forall w \in \mathcal{V}$ *such that:*

$$B(w, u) = (w, f) \tag{2.17}$$

2.1.3 The Variational Multiscale problem

Up to this point, it can only be spoken of a variational method, where the solution to the PDE's can be approximated in terms of the choice of trial functions. In order to obtain a multiscale model, a separation of the quantity u as shown in figure 2.1 must be considered.

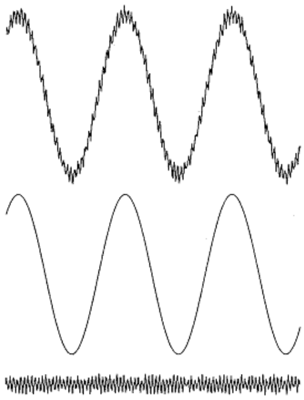

Figure 2.1: Scales separation Hughes et al. (2000)

Here, a signal is split into its large ($\overline{u}$) and small (u') components (low and high signal frequencies respectively), such that:

$$u = \overline{u} + u' \tag{2.18}$$

When decomposing the trial solutions $u \in \mathcal{S}$ and weighting functions $w \in \mathcal{V}$ according to (2.18), their spaces take the forms: $\mathcal{S} = \overline{\mathcal{S}} \oplus \mathcal{S}'$ and $\mathcal{V} = \overline{\mathcal{V}} \oplus \mathcal{V}'$ respectively. After a substitution of the separated quantities in (2.17), this variational equation now reads:

$$B(\overline{w} + w', \overline{u} + u') = (\overline{w} + w', f) \tag{2.19}$$

Noting the linear independence of $\overline{w}$ and w', assuming sufficient smoothness, and with:

$$\overline{u} = g \quad \text{on } \Gamma \quad \forall \overline{u} \in \overline{\mathcal{S}} \tag{2.20}$$
$$u' = 0 \quad \text{on } \Gamma \quad \forall u' \in \mathcal{S}' \tag{2.21}$$
$$\overline{w} = 0 \quad \text{on } \Gamma \quad \forall \overline{w} \in \overline{\mathcal{V}} \tag{2.22}$$
$$w' = 0 \quad \text{on } \Gamma \quad \forall w' \in \mathcal{V}' \tag{2.23}$$

Equation (2.19) can now be split into separate problems for the large and small scales, given by:

$$B(\overline{w}, \overline{u} + u') = (\overline{w}, f) \tag{2.24}$$
$$B(w', \overline{u} + u') = (w', f) \tag{2.25}$$

In general, the small-scales equation (2.25) will not be solved. Instead, a model will be developed to represent the u' in the large-scales equation (2.24), which will account for the effects of the small scales in the flow. Therefore, focus will now be turned almost exclusively to such large-scales equation. Expanding (2.24) and, for simplicity purposes, hereafter employing w to denote $\overline{w}$ yields:

$$B(w, \overline{u}) + B(w, u') - (w_x, \overline{u}u') = (w, f) \tag{2.26}$$

Now denoting as subindices the variables in which the Burgers differential operator (2.3) is expressed; the expansion (2.26) can be re-expressed in terms of such operators as:

$$(w, \mathcal{L}_{\overline{u}}\overline{u}) + (w, \mathcal{L}_{u'}u') - (w_x, \overline{u}u') = (w, f) \tag{2.27}$$

From this form, successive integration by parts of the second term, until no derivatives of the small scales exist, gives:

$$(w, \mathcal{L}_{\overline{u}}\overline{u}) + (\mathcal{L}^*{}_{u'}w, u') - (w_x, \overline{u}u') = (w, f) \tag{2.28}$$

Where $\mathcal{L}^*{}_{u'}$ represents the adjunct operator given by:

$$\mathcal{L}^*{}_{u'} = -\frac{\partial}{\partial t} - \frac{u'}{2}\frac{\partial}{\partial x} - \nu\frac{\partial^2}{\partial x^2} \tag{2.29}$$

Two important assumptions will now be made. First, that the small scales respond instantaneously to changes in the large scales motions, i.e. quasi-static behavior of u' is assumed. Work by Codina et al. (2007) has incorporated the use of ODE's to achieve a dynamic representation of such scales, however, this framework will not be incorporated at this stage of this research. Second, that the testing functions will be piecewise linears thus having a zero second derivative. These assumptions allow neglecting the fist, and last terms of (2.29). In this way, the variational multiscale version of the problem is finally given by:

Find $u \in \mathcal{S} \quad \forall \overline{w} \in \overline{\mathcal{V}}$ *such that:*

$$B(\overline{w}, \overline{u}) - \left(\overline{w}_x, \frac{u'^2}{2}\right) - (\overline{w}_x, \overline{u}u') = (\overline{w}, f) \tag{2.30}$$

2.2 A brief DNS exploration

Given the relative simplicity of this equation, performing DNS computations which will capture the behavior of the boundary layer is possible. In this situation, the effects of the small scales u' can be neglected under the assumption that the whole range of motion scales is captured by $\overline{u}$. This section presents a quick exploration of the Burgers equation in terms of DNS computations, same which will later be employed as reference data for the SGS models design.

2.2.1 Theoretical and computational verifications

Initially, a quick verification of the theoretical formulation and code implementation, is made through an order of accuracy test, which verifies the $O(\Delta x^2, \Delta t^2)$ convergence of the computed solutions towards the exact solution. While such exact solution might not always be available from reference data, the method of manufactured solutions (MMS) can be employed for this purpose, same which will be briefly explained now.

The Method of Manufactured Solutions

The MMS [Roache (2002); Roy (2005)] provides a way to generate reference exact solutions to a PDE in a predetermined domain. Instead of computing a solution to the model equation, one assumes a “target” solution and designs a source term which should bring the model to generate such solution. For the case of the Burgers equation, this is done as follows:

Starting from:

$$\frac{\partial u}{\partial t} + u\frac{\partial u}{\partial x} = \nu\frac{\partial^2 u}{\partial x^2} + f(x,t) \tag{2.31}$$

In the domain $\Omega = [0, \pi]$, a target (manufactured) solution $u_m = sin(x)cos(t)$ is assumed. Substitution of u_m in (2.31) allows finding a forcing term $f(x,t)$ which satisfies the equation. For this particular case, it results in:

$$f(x,t) = -sin(x)sin(t) + sin(x)cos(x)cos^2(t) + \nu sin(x)cos(t) \tag{2.32}$$

With a set of boundary and initial conditions matching the manufactured solution such as:

$$u(0,t) = u(\pi,t) = 0$$
$$u(x,0) = sin(x)$$

The numerical method can now be employed to verify that indeed, the solution of (2.31) converges with the appropriate order of accuracy to u_m.

The order of accuracy test

For this part of the verification, it is necessary to compute a form of total error in the solution, same which for this case will be the L^2 norm of the nodal error:

$$\epsilon = L^2(u) = \sqrt{\sum_{i=1}^{N_X}(u_i - u_i^{ref})^2} \tag{2.33}$$

Where N_X stands for the number of grid points, and u^{ref} represents the reference solution; in this case, the manufactured solution u_m. With the number of time steps given by N_T, a sweep for $N_T = [2, 100000]$ and $N_X = [8, 4096]$ reveals the order of accuracy of the numerical method. As it can be appreciated in figure 2.2, the test displays a good $O(\Delta x^2, \Delta t^2)$ convergence within reasonable ranges. These tests were conducted for a fixed $\Delta x = 1/1024$ in the case of the time refinement test, and a fixed $\Delta t = 0.01$ for the grid refinement sweep. It can be seen that at the lowest ranges of refinement for both tests, the minimum error achieved is dictated by the fixed values of the alternate variable, as the curves flatten to an asymptotic value of ϵ. With this reasonable indication of the effectiveness of the numerical method and coding implementation, the DNS tests can be conducted.

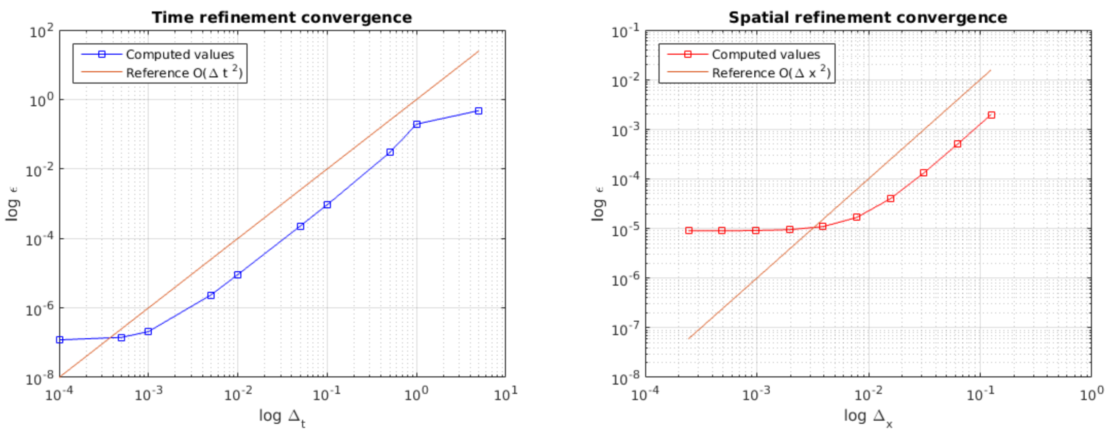

(a) Δt order of accuracy test

(b) Δx order of accuracy test

Figure 2.2: log-log plots of ϵ vs $\Delta(t, x)$ for convergence studies

2.2.2 The DNS results

Without unresolved scales, given the resolution of the grid, the problem takes the form of (2.17), for which the domain of computation will (unless otherwise specified) henceforth be: $\Omega = [0, 1]$. An initial run is done for a grid of $N_{DNS} = 4096$ nodes and a total time of $T_{DNS} = 10s$ where:

$$\begin{aligned} Re = 100, \quad f = 1.0, \quad \Delta t = 0.01s \\ u(0,t) = u(1,t) = 1.0 \\ u(x,0) = 1.0 \end{aligned}$$

A transient solution is shown in figure 2.3, which evidences a phenomenon of "wave steepening", along with a clear boundary layer development, characterized by high gradients in the solution in the proximity of $x = 1.0$.

The relatively quick transition of the solution to a steady state is evidenced by the practical overlap of the $u(x, 1.0)$ and $u(x, 10.0)$ solutions. A quick analysis of the bulk velocity in the domain as a function of time, reveals the transient range, which will be important to determine the appropriate initial solutions for statistics computations in later studies. Figure 2.4, shows that uBulk achieves a 99.9% of its maximum value at $t = 0.77s$.

Having verified the general behavior and implementation of this formulation, the next step is to consider coarsened grids. As previously described, the focus of this research is the study of SGS in the context of realizable LES computations. The following chapter will explore the use of this methodology (VMM) in the presence of unresolved scales, introducing the essential forms of the SGS models and setting the benchmarks for the proposed modifications.

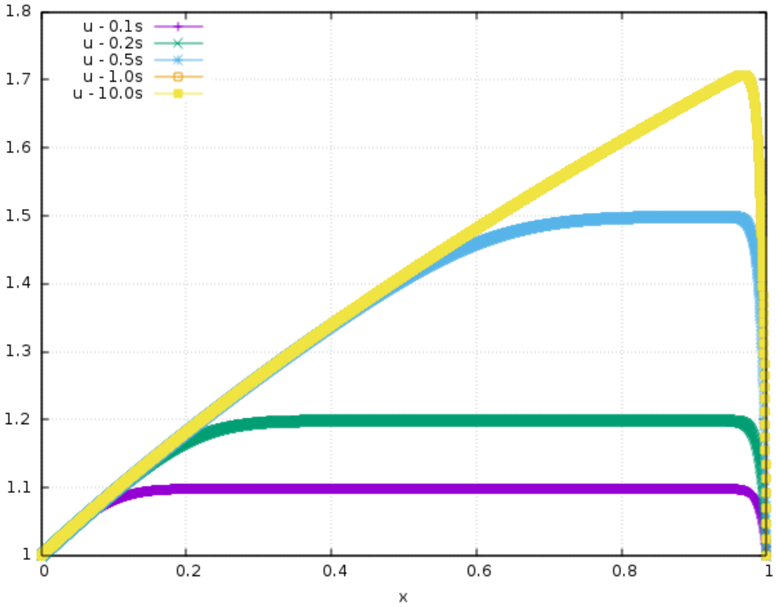

Figure 2.3: Transient DNS solution for Burgers equation

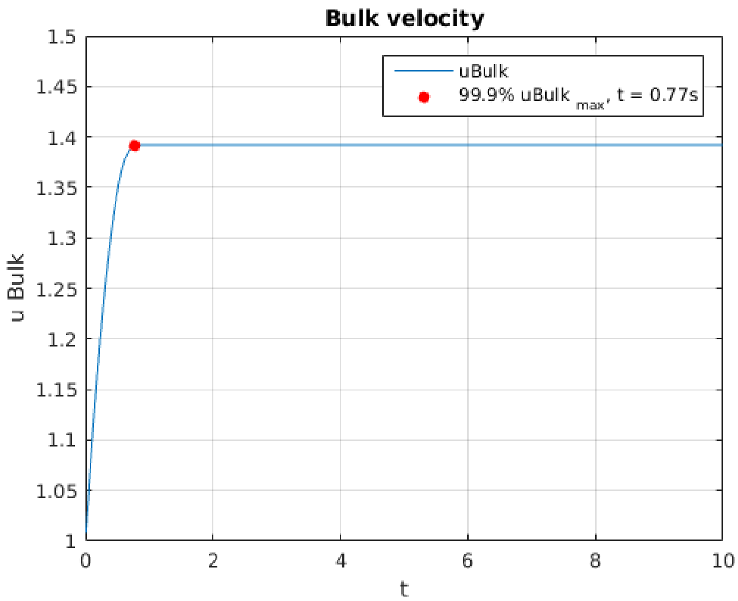

Figure 2.4: Bulk velocity

Chapter 3

The initial SGS approximations

As described before, an important feature of the Burgers equation is its nonlinear term. This term is responsible for the "wave steepening" behavior of this equation, which is absent in the linear advection-diffusion model. While these features do not represent a problem in a fully resolved flow, a coarsened grid provides a framework for unresolved scales to be present and exhibit their influence in the solution. The use of SGS models is important in this context to account for their effects and therefore, this chapter will provide an initial understanding of baseline models behavior and serve as a starting point for alternative formulations.

3.1 Solutions with $u' = 0$

Providing no approximation for the small scales is by itself not a problem, so long as the grid size allows capturing the smallest scales of motion. This scenario is a function of both the mesh spacing, and the Reynolds number. At low Re, the turbulent flow structures do not break down to very small characteristic lengths before dissipating their energy, and a coarse mesh is able to capture the smallest ranges of motion in the flow. In the context of the BE, this is analogously observed as a lack of severe wave steepening. In these scenarios, there is no need to employ u' approximations, provided that the subset of large scales solutions spans the complete solution space such that: $\mathcal{S} = \overline{\mathcal{S}}$. However, when some scales of motion (high gradients for the BE) cannot be captured by the grid anymore, the effects of the missing small scales become important and, within this framework, even appreciable in the behavior of the numerical method.

3.1.1 First LES attempts and results

A $u' = 0$ sweep for Re was simulated, given by table 3.1, where the nodal error with respect to the DNS solution is computed at steady state by (2.33) with $u_{ref} = u_{DNS}$. The nodal exactness at machine precision for $Re = 0.2$ quickly degrades with increasing Re, which is partially shown in figure 3.1. At high Re, not only the error in the solution increases, but also unphysical oscillations appear. This effect can alternatively be appreciated for a fixed Re, where a mesh coarsening produces similar effects.

Re	ϵ
0.2	0.0
1	0.00005
2	0.00034943
10	0.0077199
20	0.02323
100	0.31949
200	0.61663

Table 3.1: LES nodal error with Re for $N_X = 32$

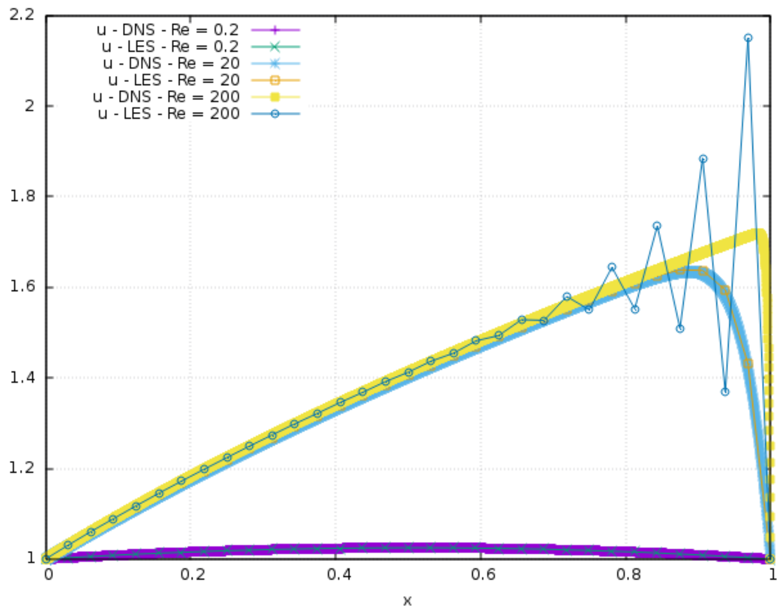

Figure 3.1: DNS vs LES solution for different Re

Table 3.2 shows the results of a similar procedure for a sweep in grid spacing. The coarsening grid quickly increases the nodal error, until eventually instabilities appear, as shown in figure 3.2. This low exactitude of the coarse-grid, high-Reynolds solutions under a $u' = 0$ approximation is therefore the motivation for SGS models which can address these issues. A representation of the small scales u' in (2.30) will serve this purpose, and a brief explanation of some basic formulations is provided now.

N_X	ϵ
512	0.0038734
256	0.011267
128	0.034082
64	0.11481
32	0.31949
16	0.61289
8	1.1768

Table 3.2: LES nodal error with N_X for $Re = 100$

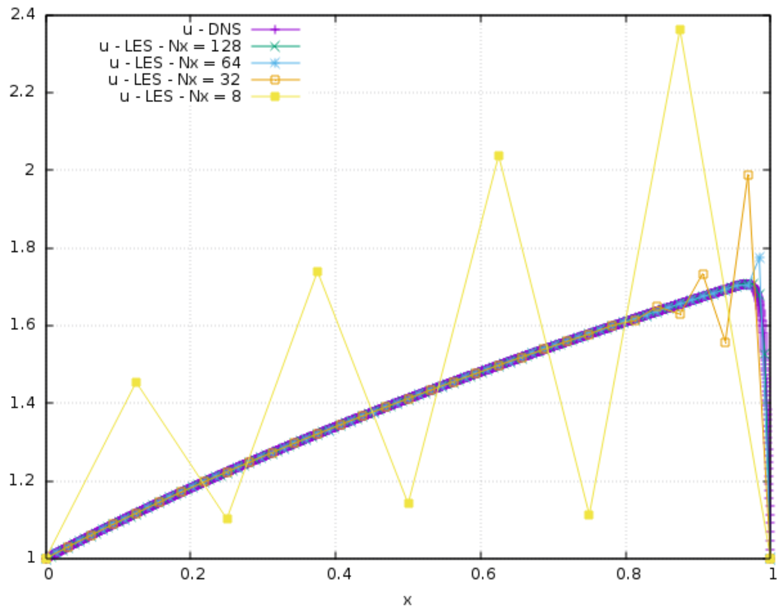

Figure 3.2: DNS vs LES solution for different N_X

3.1.2 Modeling the small scales

While (2.30) represents a problem which takes into account the effect of the small scales, these still exist explicitly in the equation. An approximation for them is required, provided that their computation is not possible in terms of reasonable resources. As proposed by Hughes (1995), such scales can be represented in terms of their element-local Green's function:

$$u'(x) = \int_{\Omega} \mathcal{G}'_e(x,y)\mathcal{R}(y)dy \tag{3.1}$$

However, such local Green's function can only be derived for linearized cases. In the presence of nonlinear behavior, as observed for the Burgers equation, an approximation can be made, making (3.1) take the form:

$$u' \approx -\tau\mathcal{R}(\overline{u}) \tag{3.2}$$

Where τ can be interpreted as an element-averaged Green's function, and $\mathcal{R}$ will be given by the residual of the large scales found through the strong form of the Burgers equation (2.1) as:

$$\mathcal{R}(\overline{u}) = \mathcal{L}\overline{u} - f \tag{3.3}$$

The relevance of having a residual-based formulation becomes evident in the regions where the large scales can describe the dynamics of the local flow. This means for example that for a wall-bounded flow, within regions of high y^+ where the turbulent structures can be (generally) expected to have large characteristic lengths, the residual of the large scales tends to zero. This means consequently that the small-scale approximation vanishes locally, therefore “automatically deactivating” the SGS away from the walls or in intermittent laminar regions, where it is not needed.

An important element in this framework is that the small-scales model in the large-scales equation will serve two purposes. As said before, the first is to incorporate the effects of the unresolved scales into the behavior of the large scales. However, as a second feature, these small-scale terms, along with their corresponding models, will serve as stabilization terms for the large-scales equation numerical solution. Previous formulations for the approximation τ have been made for example by Shakib and Hughes (1991), which in basic form reads:

$$\tau = \tau(a, h, \nu) \tag{3.4}$$

Where h represents the mesh size, and a the (constant) element local large-scale convection velocity. With (3.3), and (3.4), now the small scales in (2.30) can be replaced by (3.2), and the variational multiscale problem becomes an exclusive function of the large scales which can now be written as:

Find $\overline{u} \in \overline{\mathcal{S}} \quad \forall \overline{w} \in \overline{\mathcal{V}}$ *such that:*

$$B(\overline{w}, \overline{u}) - \left(\overline{w}_x, \frac{(\tau\mathcal{R})^2}{2}\right) + (\overline{w}_x, \overline{u}\tau\mathcal{R}) = (\overline{w}, f) \tag{3.5}$$

From here to be noted that the trial solution space has been reduced to the large scales subspace, provided that the u' has now been modeled. It is therefore in approximations like (3.4) where the quality of the small scales reconstruction resides. A “perfect” τ would provide a nodally exact reconstruction, regardless of the mesh coarseness, and such formulation would be the ideal goal of this research. However, a realistic approach aims to improve the currently available SGS models, while at the same time feeding them with reference data in an attempt to obtain a formulation which can serve as a coupling term for a hybrid method. A baseline approximation is now presented, which will serve as starting line for the later proposed modifications.

3.2 Shakib's stabilization formulation

Based on Hughes et al. (1986), Shakib and Hughes (1991) developed a definition for τ for a one-dimensional linear scalar advection-diffusion model problem. It is based on an approximation of the exact volume averaged Green's function for the linear problem. This stabilization term can be applied to model the small scales in the Burgers equation keeping in mind the influence of the nonlinearity in its effectiveness. This section will provide a quick review of this formulation and a quick analysis of its effectiveness in modeling the subgrid scales within the LES environment in the Burgers equation.

3.2.1 The τ formulation

The time-dependent problem for linear advection-diffusion is given in short notation by:

$$u_t + a u_x = \nu u_{xx}, \quad \text{for} \quad x \in \Omega, \quad t > 0 \tag{3.6}$$

Where a stands for the advective speed, and ν for a coefficient of diffusivity, which for our purposes will henceforth be treated as the kinematic viscosity. A stabilization term for the small scales of the time-dependent problem is given by:

$$\tau = \left[\left(\frac{2}{\Delta t} \right)^2 + \left(\frac{2a}{\Delta x} \right)^2 + 9 \left(\frac{4\nu}{\Delta x^2} \right)^2 \right]^{-1/2} \tag{3.7}$$

Which can easily be converted for the steady-state of (3.6) taking the limit as $\Delta t \to \infty$, thus becoming:

$$\tau = \left[\left(\frac{2a}{\Delta x} \right)^2 + 9 \left(\frac{4\nu}{\Delta x^2} \right)^2 \right]^{-1/2} \tag{3.8}$$

The use of this simple form of τ in (3.2) provides some insight as to which path will be followed in attempts to obtain more effective approximations, and an understanding of its potential usefulness to couple the RANS/LES methods. The next subsection provides a quick exploration in the context of the Burgers equation problem.

3.2.2 Initial tests on the Burgers equation

A test case for Shakib's τ formulation is set up for the Burgers equation problem as given by (3.5), (3.2), and (3.8) in an $\Omega = [0, 1]$ domain. Employing the parmeters:

$$Re = 1000, \quad N_{X_{DNS}} = 2048, \quad N_{X_{LES}} = 8$$
$$u(0,t) = u(1,t) = 1.0$$
$$u(x,0) = 1.0$$

A sweep for the forcing term was done according to table 3.3. The increasing nonlinearity introduced by a growing forcing term provides an insight of the limitations of Shakib's formulation, which as said before, has been designed using linear advection-diffusion problems. An estimation of the normalized steady-state nodal error is given by:

$$\epsilon = \frac{1}{(u_{DNS_{max}} - 1.0)} \sqrt{\sum_{i=1}^{N_{X_{LES}}} (u_i - u_{DNS_i})} \tag{3.9}$$

While the formulation is able to stabilize the numerical method, its ability to reproduce the small scales in the proximity of the boundary layer, and therefore its near-wall effectiveness decreases with increasing nonlinearity. As shown in figures 3.3 and 3.4 the growth of the error of the sweep is mostly originated in the proximity of the $x = 1.0$ wall, where the boundary layer induces large gradients.

$f(x,t)$	ϵ
0.01	0.0081054
0.1	0.012347
1.0	0.033054
2.0	0.042497
5.0	0.055114

Table 3.3: LES nodal error with $f(x,t)$ for $Re = 1000$

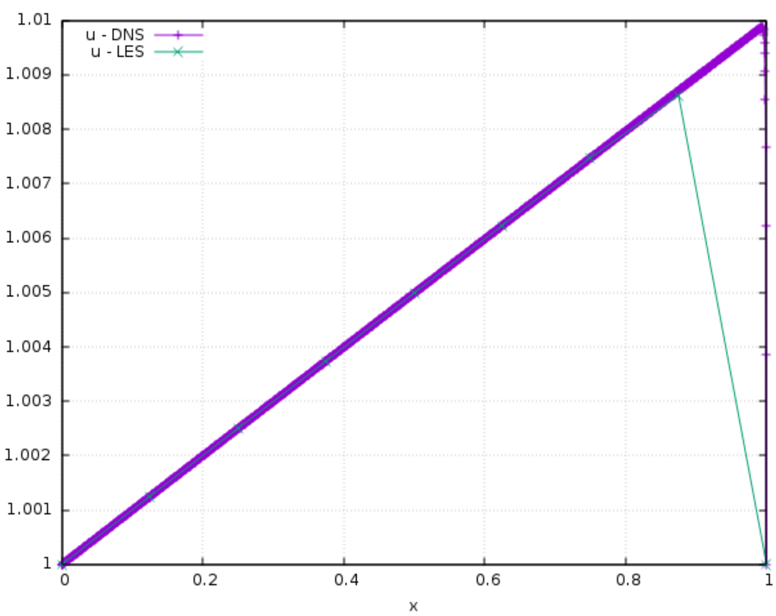

Figure 3.3: DNS vs LES solution for $f(x,t) = 0.01$

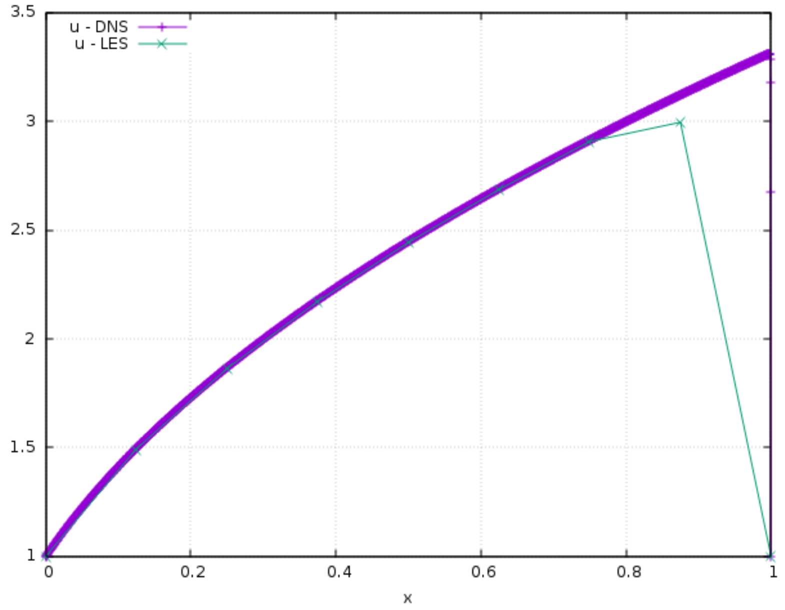

Figure 3.4: DNS vs LES solution for $f(x,t) = 5.0$

3.3 Comments

This chapter has evidenced the capabilities of a basic existing SGS model. With an awareness of its limitations, a variety of approaches will be now addressed in an attempt to improve its capabilities. At the same time, such approaches will be based on the use of reference data which as will be explained later, is employed to obtain more exact solutions. The advantage of employing such reference data is that this makes the model intrinsically responsive to the statistical behavior of the flow. In this way, an effective coupling of RANS and LES methods can be made through the modified SGS model. Additionally, attention will be also focused on the adjustability of the small-scales approximations, and consequently, on the authority that they will exert on the overall behavior of the flow. This, provided that it becomes unpractical to model all the unresolved scales behaviors in the NSE case.

Chapter 4

Improved SGS approximations

While it has been shown that a formulation by Shakib et al. (1991) provides a good small-scales approximation to some extent, it has also been shown that its limitations become evident in the presence of increasing nonlinarity. This chapter will provide alternative formulations to the u' in an attempt to obtain improvement in dealing with the nonlinear part of the problem. A first approach is to modify the original Shakib formulation for τ such that it better resembles the upwind functions of nonlinear problems. This is done by generating better approximations to the local Green's function from where they are derived. A second approach, introduces an additional term for u', such that the linear and nonlinear components of the flow can be handled separately. We employ a response surface approach to investigate the influence of their parameters. These also give an indication of the viability of Goal-Oriented or Artificial Neural Networks approaches for improving the representations of unresolved scales using the mean flow reference data.

4.1 The local Green's function approach

4.1.1 The local Green's function

Starting from the small scales equation (2.25), a model for u' can be derived in the following way. Rewriting this equation as:

$$B(w', \overline{u}) + B(w', u') - (w'_x, \overline{u}u') = (w', f) \tag{4.1}$$

and noting that under appropriate boundary conditions (2.21, 2.23), the equivalence for arbitrary variables a and b:

$$B(a, b) = (a, \mathcal{L}b) \tag{4.2}$$

can be assumed to hold for the strong and weak Burgers operators given by (2.3), and (2.16) respectively. The small-scales equation can be written as:

$$B(w', u') - (w'_x, \overline{u}u') = -(w', \mathcal{L}\overline{u} - f) \tag{4.3}$$

Which for a linearization of the Burgers operator (2.3) around $\overline{u}$, here denoted as $\mathcal{L}_{\overline{u}}$, becomes:

$$(w', \mathcal{L}_{\overline{u}}u') = -(w', \mathcal{R}) \tag{4.4}$$

Where $\mathcal{R}$ stands for the residual of the large scales. This implies:

$$\mathcal{L}_{\overline{u}}u' = -\mathcal{R} \tag{4.5}$$

By setting up a Green's function problem, the small scales can be found as a response to the large-scales residual and the initial conditions. As shown by Edeling (2011), an analytic solution for the element-local Green's function $\mathcal{G}'_e$ can be obtained for a given $\overline{u}$ under a steady Burgers case as:

$$\mathcal{G}'_e(x,y) = \begin{cases} -C_1(y)\left(\frac{\gamma\sqrt{\pi}}{Re}\right)\beta_{i-1}(x)exp\left[\gamma^2 h^{-2}(\Delta\overline{u}x + \overline{u}_{i-1}h)^2\right] & 0 \leq x < y \\ -C_2(y)\left(\frac{\gamma\sqrt{\pi}}{Re}\right)\beta_{i}(x)exp\left[\gamma^2 h^{-2}(\Delta\overline{u}x + \overline{u}_{i-1}h)^2\right] & y \leq x \leq h \end{cases} \tag{4.6}$$

Where C_1, and C_2 are given by:

$$C_1(y) = \frac{-Re\beta_i(y)}{erf(\gamma\overline{u}_i) - erf(\gamma\overline{u}_{i-1})}$$
$$C_2(y) = \frac{-Re\beta_{i-1}(y)}{erf(\gamma\overline{u}_i) - erf(\gamma\overline{u}_{i-1})}$$

And β_i, β_{i-1} by:

$$\beta_{i-1}(x) = erf(\gamma\overline{u}_{i-1} - erf(h^{-1}\gamma(\Delta\overline{u}x + u_{i-1}h))$$
$$\beta_{i}(x) = erf(\gamma\overline{u}_{i} - erf(h^{-1}\gamma(\Delta\overline{u}x + u_{i-1}h))$$

Where $erf(\cdot)$ sands for the error function, $\Delta\overline{u} = \overline{u}_i - \overline{u}_{i-1}$, and γ is defined as:

$$\gamma = \left(\frac{-hRe}{2\Delta\overline{u}}\right)^{\frac{1}{2}}$$

With (4.6), the element-averaged value τ is computed as:

$$\tau = \frac{1}{h}\int_{\Omega_e}\int_{\Omega_e} \mathcal{G}'_e(x,y)dxdy, \quad x,y \in \Omega_e \tag{4.7}$$

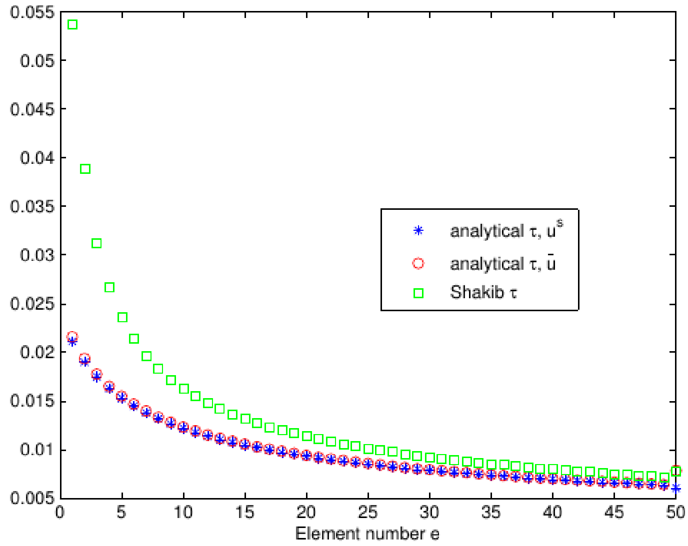

Figure 4.1: Comparison of different τ formulations by Edeling (2011)

Which can be substituted in (3.2) to obtain the approximation of the small scales for the large-scales problem. A comparison of this formulation and Shakib's approximation of τ given by (3.8) is also done by Edeling (2011) and shown in figure 4.1 for a forcing term $f = 1.0$; displaying the differences in the outcome of the τ function.

Ideally, the formulation of τ should approach the element-averaged analytic solutions of $\mathcal{G}'_e$. In an attempt to achieve this, a free coefficient formulation of (3.8) is introduced, which when optimized, allows such solutions to be resembled, as will be explained now.

4.1.2 Optimization of the local Green's function

An initial approach to an improvement of the stabilization model is based on its steady state response to variations in its coefficients. A related approach was initially explored by Albrecht (2013) through a Goal-Oriented optimization; attempting the minimization of a goal functional while employing a trust-region based conjugate gradient method by Steihaug (1983) to make the LES model match available RANS data. However, some distinctions must be pointed out to justify this approach:

- The formulation considered an SGS approximated by a SUPG operator rather than a VMM approach.
- While the CG method procedure allows finding the optimized coefficients, it provides little or no information about the solution space where they reside. For the purposes of this thesis, the shape of the solution space is important to understand the behavior of the small-scales approximation, and its future modifications.

With these distinctions pointed out, an attempt of improvement was based on a simple modification of the original Shakib formulation (3.8). Introducing a free-coefficient form given by:

$$\tau = \left[\gamma_1 \left(\frac{a}{\Delta x} \right)^2 + \gamma_2 \left(\frac{\nu}{\Delta x^2} \right)^2 \right]^{-1/2} \tag{4.8}$$

Where it is worth noting that the coefficients for a and ν inside the square terms have now been incorporated to γ_1 and γ_2 respectively. This approach is also considered by Chen et al. (2015) to adjust the u' approximation for a POD basis. Under this representation, the original coefficients in Shakib's formulation take the values of: $\gamma_1 = 4.0$ and $\gamma_2 = 144.0$. As said before, the investigated method relies on reference data, for which the benchmark case will be given by:

$$\begin{aligned} Re = 100, \quad f = 1.0, \quad N_{X_{DNS}} = 1024, \quad N_{X_{LES}} = 8 \\ u(0,t) = u(1,t) = 1.0 \\ u(x,0) = 1.0 \end{aligned}$$

After a run for both the DNS and LES resolution, figure 4.2 shows the stabilized LES solution with the original Shakib coefficients. The error between both solutions as computed by (3.9) is $\epsilon = 0.044827$, which once again, derives mainly from the LES node in the nearest proximity of the boundary layer.

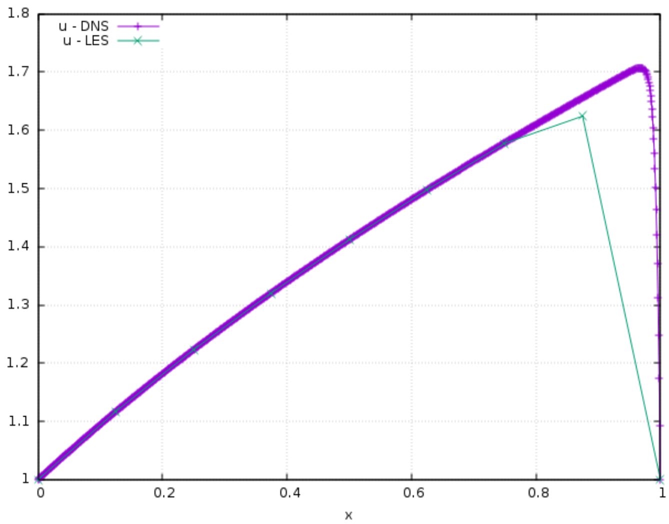

Figure 4.2: DNS vs LES solution for $\gamma_1 = 4.0$ and $\gamma_2 = 144.0$

The optimization procedure

From the DNS data provided by the baseline run, the next step was to extract the nodal data corresponding to the LES grid. Making the assumption:

$$\overline{u} = u_{LES} \tag{4.9}$$

From where $\mathcal{R}$ can be estimated and substituted along with $\overline{u}$ into (3.5). For a given f, the residual of the weak form $\mathcal{R}_w$ can be computed for any given τ, allowing to measure an error given by the time averaged L^2 norm of $\mathcal{R}_w$, hereafter called the **Training norm**, such that:

$$\epsilon_{tr} = \frac{1}{N_T} \sum_{j=1}^{N_T} \sqrt{\sum_{i=1}^{N_X} \mathcal{R}_{w_i}^2} \tag{4.10}$$

This training norm is advantageous in that it can be done without performing a simulation [Durieux (2015)]. Under this conditions, any new form of τ can be evaluated so that $\epsilon_{tr} = \epsilon_{tr}(\tau)$ or more specifically under (4.8), $\epsilon_{tr} = \epsilon(\gamma_1, \gamma_2)$. A response surface shown in figure 4.3 is obtained for a sweep in the values of γ_1 and γ_2 in an attempt to find a combination of these which minimizes the outcome of (4.10). Such sweep is given then by:

$$\begin{aligned}
Re = 100, \quad f = 1.0, \quad N_{X_{DNS}} = 1024, \quad N_{X_{LES}} = 8 \\
u(0,t) = u(1,t) = 1.0 \\
u(x,0) = 1.0 \\
\gamma_1 = [0.0, 6.0], \quad \gamma_2 = [0.0, 1000.0]
\end{aligned}$$

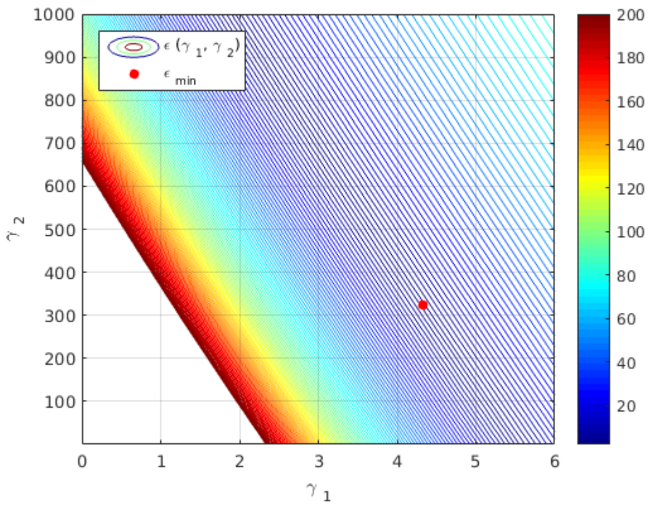

Figure 4.3: Training norm response surface for γ_1, γ_2

The minimum value for the training norm (4.10) in this case is found to be $\epsilon_{tr} = 1.1733$ at $\gamma_1 = 4.32$, and $\gamma_2 = 325.1$. While the surface seems to have a "corridor" of minimum values, seen as a diagonal from top-left to bottom-right in figure 4.3, it is worth noting that there is a variation of ϵ_{tr} along this line. Provided that it is very small compared to the variation in other directions the visual results seem to suggest an optimal line which in reality, is indeed a point for this sweep.

4.1.3 Results

Once the optimal values for the free coefficients have been established, a simple re-evaluation of the LES solution under the improved stabilization formulation can be made. Figures 4.4, and 4.5 show a comparison of the results under the standard and optimized formulations of (4.8).

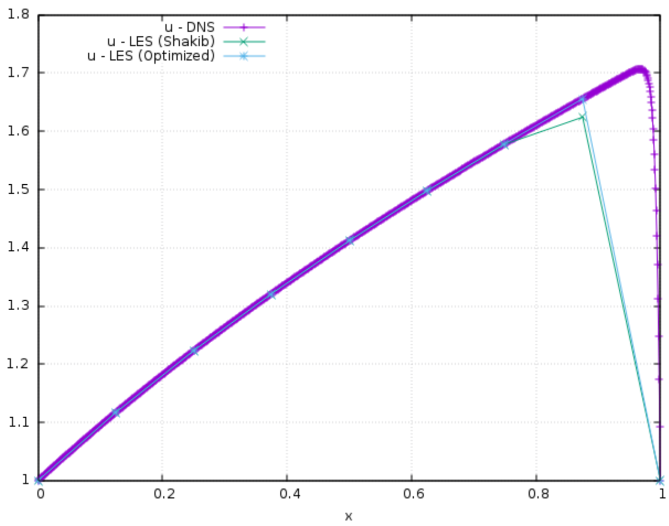

Figure 4.4: DNS vs LES solutions for standard and optimized Shakib formulations of τ

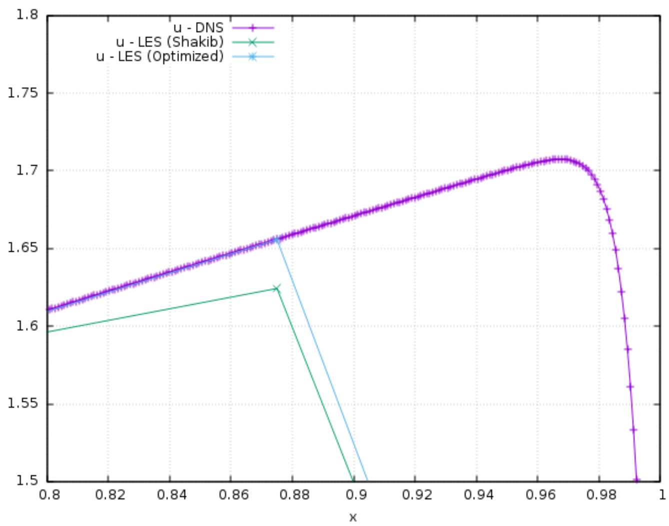

Figure 4.5: DNS vs LES solutions for standard and optimized Shakib formulations of τ (detail)

A notable improvement can be seen in the proximity of the boundary layer for the LES solution. As said before, this derives from the adjustment of the local Green's function approximation under the given conditions. While the adaptations found for γ_1 and γ_2 make the model capable to deal with the case-specific non-linearities, it is worth remembering that the original Shakib formulation (3.8) was designed for linear advection-diffusion. This means that by itself, it is capable of providing unresolved scales modeling for the linear "aspects" of the flow. Rather than case-specifically adapting it, an alternate approach is the introduction of a second term capable of handling such non-linearities. The following section provides a second approach to achieve improvements in the SGS models while preserving the original form of Shakib's τ formulation.

4.2 The asymptotic expansion approach

4.2.1 Scovazzi's fine-scale approximation

An alternate approach to the representation of the small-scales by Scovazzi (2004), is to consider u' as given by the asymptotic expansion:

$$u' = \varepsilon u'_1 + \varepsilon^2 u'_2 + \varepsilon^3 u'_3 + ... = \sum_{n=1}^{\infty} \varepsilon^n u'_n \tag{4.11}$$

Where $\varepsilon = ||\mathcal{R}||$. Now, consider a redefinition of the weak Burgers operator (2.16) to be given as:

$$B(w,u) = B_1(w,u) + B_2(w,u,u) \tag{4.12}$$

Where the bilinear and trilinear forms $B_1(\cdot,\cdot)$, and $B_2(\cdot,\cdot,\cdot)$ are given by:

$$B_1(w,u) = (w,u_t) + (w_x, \nu u_x) \tag{4.13}$$

$$B_2(w,u,v) = -\left(w_x, \frac{uv}{2}\right) \tag{4.14}$$

Furthermore, assume a linearization of the weak burgers operator (2.16) around $\overline{u}$ which redefines it as:

$$B_{\overline{u}}(w,u) = B_1(w,u) + B_2(w,u,\overline{u}) + B_2(w,\overline{u},u) \tag{4.15}$$

It can be seen that the small-scales equation (4.3) can easily be re-expressed for this operators as:

$$B_{\overline{u}}(w',u') + B_2(w',u',u') = (w',\mathcal{R}) \tag{4.16}$$

A substitution of the asymptotic expansion (4.11) into this form of the small-scales equation yields:

$$\sum_{n=1}^{\infty} \varepsilon^n B_{\overline{u}}(w',u'_n) + \sum_{n=2}^{\infty} \varepsilon^n \sum_{j=1}^{n-1} B_2(w',u'_j,u'_{n-j}) = (w',\mathcal{R}) \tag{4.17}$$

Which produces the system of equations given by:

$$B_{\overline{u}}(w', u_1') = \left(w', \frac{\mathcal{R}}{\varepsilon}\right), \quad \text{when } n = 1 \tag{4.18}$$

$$B_{\overline{u}}(w', u_n') = -\sum_{j=1}^{n-1} B_2(w', u_j', u_{n-j}'), \quad \text{when } n \geq 2 \tag{4.19}$$

Now $B_{\overline{u}}$ can be inverted through a Green's function as detailed in section 4.1. While this representation is intended to progressively solve the terms of the expansion in finer embedded grids, eventually this will resemble a QDNS formulation, which as explained before, is to be avoided. Instead, the asymptotic expansion form is employed now to introduce additional terms, capable of dealing with the nonlinearities in ways in which the Green's function approximation falls short.

4.2.2 Optimization of an expression for u'

Following this logic, the approximation of the unresolved scales will now incorporate a second term, such that:

$$u' \approx u_1' + u_2' = -\tau\mathcal{R} + \eta\varphi\mathcal{R}^2 \tag{4.20}$$

Where η is a function which enforces dimensional consistency based on the local grid spacing h and a reference velocity U_{ref}, thus given by:

$$\eta = \frac{h^2}{U_{ref}^3} \tag{4.21}$$

The formulation of η was designed keeping in mind that there is a relationship between the solution gradients $\overline{u}_x$ and the local $\mathcal{R}^2$ terms. This means that, for example, an η design which could incorporate $\overline{u}_x$ in its denominator, would cause a difficulty for the action of u_2'. This last originates from the fact that in regions of high gradients, η would attempt to minimize u_2', while $\mathcal{R}^2$ would attempt to increase its effect, thus mutually interfering. For the tested cases, where the grid spacing h is constant, η was observed to become a constant scaling parameter. A large advantage of this formulation is that it naturally reverts to a $u' \approx -\tau\mathcal{R}$ approximation in regions of weak nonlinearity, where $\mathcal{R}$ is small. Shakib's τ is known to work well for weak nonlinearities so it is used to define the τ in (4.20).

Additionally $\varphi = \varphi(x)$ represents a distribution function intended to further localize the effects of u_2', to areas of strong non-linearity. A natural choice for a distribution function $\varphi(x)$ would be one which can focus the effects of the u_2' term to those areas which are expected to require additional modeling. For this case, this is particularly important in the boundary layer, where as seen in figure 4.2, a u_1' approximation based on Shakib's τ (3.8) is not enough to handle the non-linearities in the proximity of $x = 1.0$. Given that the form for the second term this expansion is based on simple assumptions, it is necessary to localize it to its regions of validity. Given that the mid channel region is already reasonably approximated by the LES under the exclusive stabilization of u_1', it is also of interest to keep those areas of the domain unaffected. Two mechanisms ensure this purpose is being served, first, and as here explained, the distribution function will keep u_2' inactive in the center channel. But additionally, the low gradients of this region make the solution $u \approx \overline{u}$, meaning that the LES is almost nodally exact and therefore the residual of the large-scales $\mathcal{R}$ remains small. Having this value squared in the formulation of u_2' naturally handles the vanishing of the second therm in the asymptotic expansion within regions where the flow is well resolved, i.e. away from the boundary layer.

In the context of a model optimization it is natural to introduce free parameters which will be able to modify $\varphi(x)$, such that case-specific flexibility is introduced. With this in mind, a proposed formulation for this case is the curve given by:

$$\varphi(x) = \gamma_3(1.0 - x)x^{\gamma_4} \tag{4.22}$$

For which a variation of γ_4 provides a concentration of the function towards the boundary layer, as shown in figure 4.6. As it can be seen, under this formulation, the amplitude of the distribution function decreases with increasing γ_4. To maintain a uniform "height" of $\varphi(x)$, a normalization parameter based on the height of the curve is introduced.

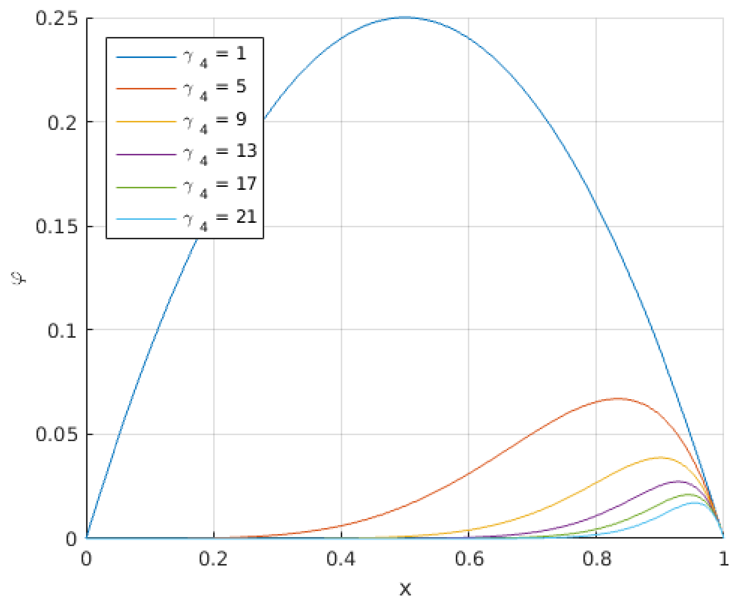

Figure 4.6: u_2' Distribution function for different γ_4

With the derivative of the distribution function equated to 0, the coordinate of maximum $\varphi(x)$ is given by:

$$\frac{d\varphi(x)}{dx} = \gamma_3[\gamma_4 x^{\gamma_4 - 1} - (\gamma_4 + 1)x^{\gamma_4}] = 0 \tag{4.23}$$

Which yields:

$$\varphi(x)_{max} = \varphi(x)\Big|_{\left(\frac{\gamma_4}{1+\gamma_4}\right)} \tag{4.24}$$

Therefore, the normalized version of $\varphi(x)$ for a base height of 1, becomes:

$$\varphi(x) = \frac{\gamma_3(1.0-x)x^{\gamma_4}}{\left(\frac{\gamma_4}{1+\gamma_4}\right)^{\gamma_4} - \left(\frac{\gamma_4}{1+\gamma_4}\right)^{\gamma_4+1}} \tag{4.25}$$

Now, as shown in figure 4.7, the amplitude of the curve is constant for any given γ_4 and its scaling is linearly dependent on γ_3.

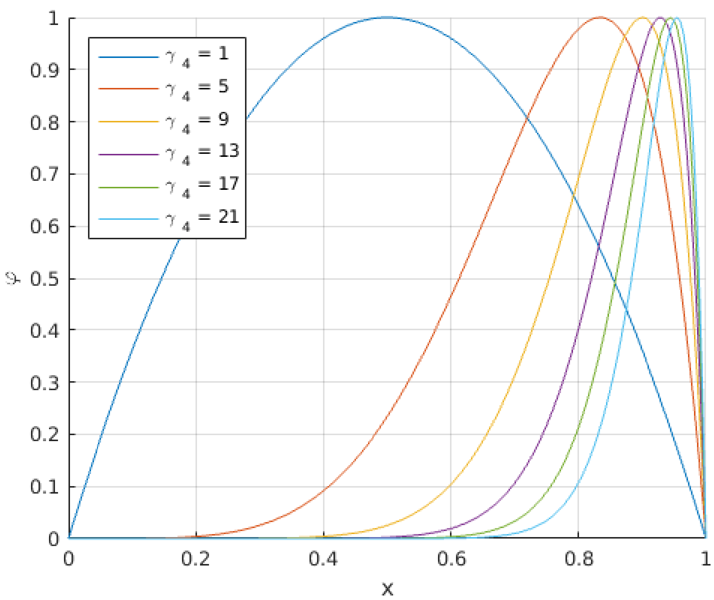

Figure 4.7: u_2' Normalized distribution function for different γ_4

4.2.3 Results

An optimization procedure similar to the one described in 4.1.2 allows pinpointing the combination of parameters γ_3, and γ_4 which will minimize the training norm as described by (4.10). Given that Shakib's formulation of τ allows for a proper handling of the stabilization in regions of linear behavior, its original form as given by (3.8) is employed for u_1', which prevents the optimization procedure from becoming a four dimensional problem.

Recalling the logic of the benchmark case, an optimization run was done for a sweep of γ_3, and γ_4 with a problem defined by:

$$\begin{aligned}
Re = 100, \quad f = 1.0, \quad N_{X_{DNS}} = 1024, \quad N_{X_{LES}} = 8\\
u(0,t) = u(1,t) = 1.0\\
u(x,0) = 1.0\\
\gamma_1 = 4.0, \quad \gamma_2 = 144.0\\
\gamma_3 = [-50.0, 50.0], \quad \gamma_4 = [1.0, 600.0]
\end{aligned}$$

A response surface shown in figure 4.8 can be obtained for the training norm. The values returned from the minimum norm evaluation are given by $\gamma_3 = -25.0$, and $\gamma_4 = 238.0$. A comparison of solutions is shown in figures 4.9, 4.9 for an unresolved scale approximation given by a γ_3, γ_4 optimized u'. It is evident that the optimized coefficients plugged into (4.20) provide an improved representation of the boundary layer phenomena.

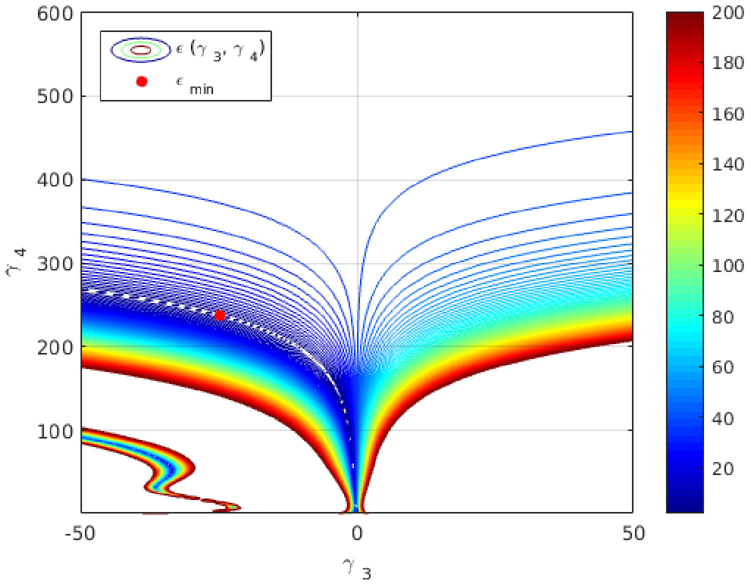

Figure 4.8: Training norm response surface for γ_3, γ_4

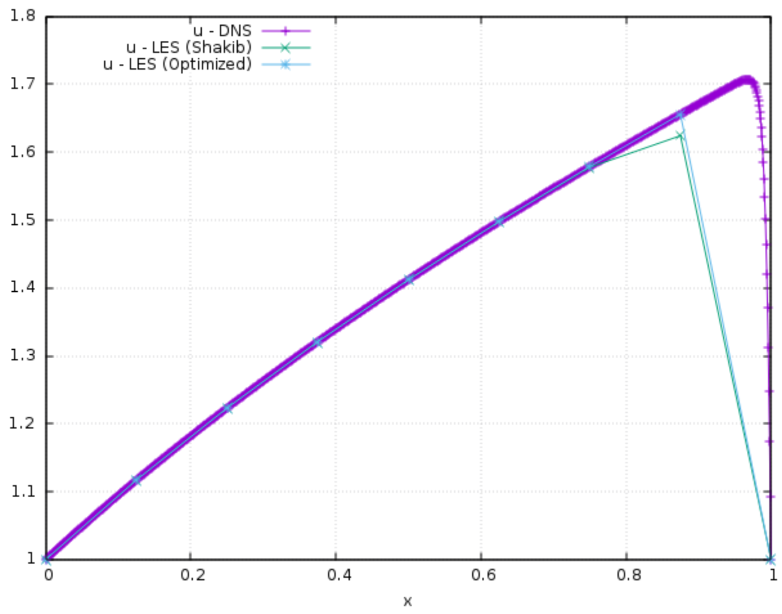

Figure 4.9: Comparison of unoptimized and optimized LES solutions.

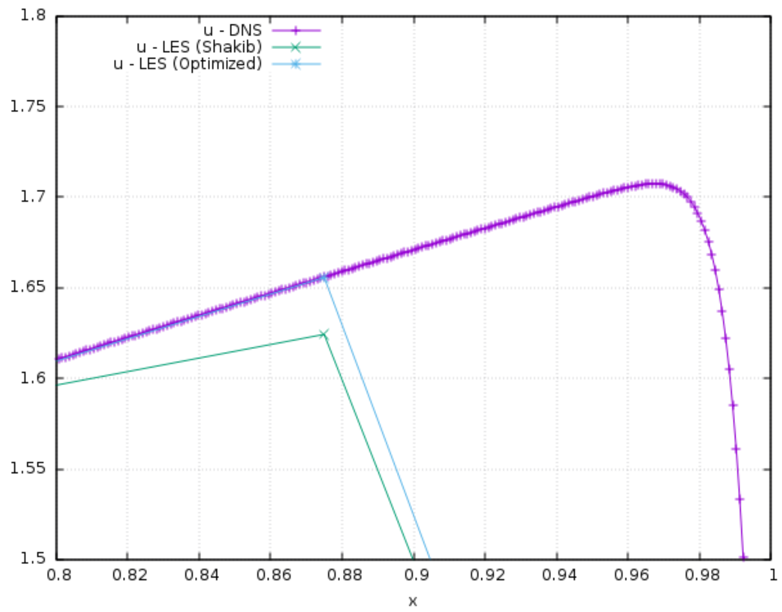

Figure 4.10: Comparison of unoptimized and optimized LES solutions. (detail)

Figure 4.12 additionally plots the distribution function as given by (4.25) under the resulting optimized values of γ_3, γ_4. The term $+1.7$ has been employed for visualization purposes, but is otherwise inexistent in the formulation. It provides a clear picture of the region of influence of the u_2' term, which is almost exclusively the boundary layer. As said before, the purpose of localizing this term to regions of elevated nonlinear behavior is to provide the additional model only where it is appropriate, in this case, the high gradients of the near wall region require the corrections provided by u_2'.

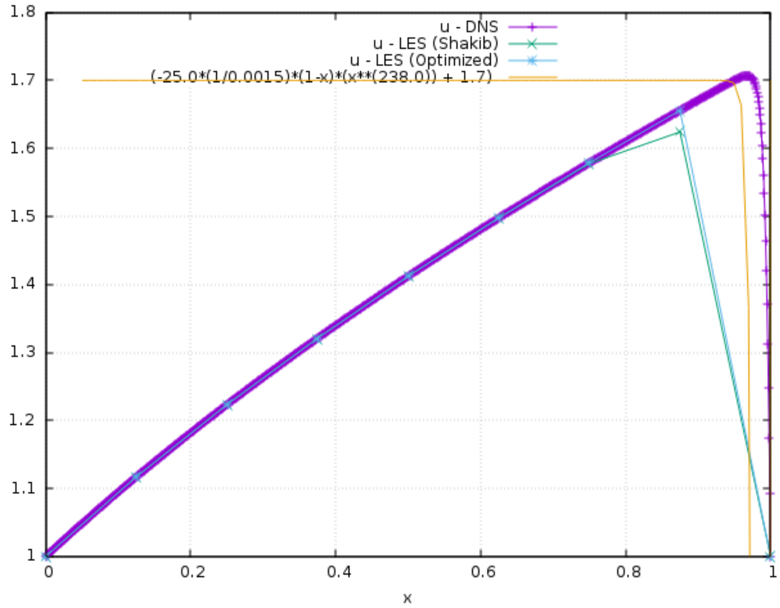

Figure 4.11: Training norm response surface for γ_3, γ_4

4.3 A brief comparison of results

While both stabilization optimization methods yield enhanced unresolved scale representations, it is worth making a brief comparison of the end results under different testing conditions. Based on the benchmark case, a series of optimization runs were made for a sweep of forcing terms for:

$$\begin{aligned} Re &= 100, \qquad N_{X_{DNS}} = 1024, \quad N_{X_{LES}} = 8 \\ u(0,t) &= u(1,t) = 1.0 \\ u(x,0) &= 1.0 \\ f &= [0.01, 5.0] \end{aligned}$$

The results of these runs are shown in table 4.1 and a few remarks can be made about them:

- As expected, low values of the forcing term introduce small non-linearities which in a general sense can be well handled by Shakib's formulation. However, nodal exactness at machine precision is achieved by the optimized formulations for a $f = 0.01$ term.

- An asymptotic expansion representation of the unresolved scales u' shows a consistent superiority even above an optimized formulation of Shakib's τ. This is explained by the presence of the distribution function and detailed below.

	ϵ x 10^{-3}				Improvement		Coefficients			
f	US	SS	OS	OE	SS to OS	OS to OE	γ_1	γ_2	γ_3	γ_4
5.0	5933	136.97	7.95	7.83	94%	2%	5.45	19	-50	325
2.0	2347	61.44	1.93	1.72	97%	11%	4.9	211	-62	301
1.0	1177	31.71	0.5	0.4	98%	16%	4.32	325.1	-25	238
0.1	118.5	3.04	0.21	0	93%	100%	2.2	583	-148	232
0.01	11.85	0.3	0	0	100%	0%	3.4	357	-188	139

Table 4.1: Comparison of LES nodal errors vs reference DNS data for: unstabilized - US; standard Shakib - SS; optimized Shakib - OS; optimized expansion - OE; and coefficient values for the optimized formulations.

The importance of the distribution function

A highly zoomed detail of the nodal behavior in the near wall region is shown by figure 4.12. While both formulations perform very well, a slight superiority of the asymptotic expansion is appreciable. A wider inspection reveals a similar tend in nodes far from the wall, as shown in figure 4.13, where for the center channel, a consistent improved performance can be seen. This behavior stems from the fact that while the u' expansion is able to act more locally, due to its distribution function and $\mathcal{R}^2$ factor, while the optimized Green's function approach affects every node in the domain. Thus, while in the latter case, a good nodal exactness is achieved in the near-wall region, it comes at a cost for the free shear flow regions. Appreciable also in figure 4.13, this fact manifests as a loss of exactness from the unoptimized Shakib formulation to the optimized Shakib formulation for the $x = 0.5$ node. On the other hand, the use of the distribution function and $\mathcal{R}^2$ allow the expansion to have negligible effects in this region, where very low non-linearity is present. In this case, the original Shakib stabilization behavior is recovered away from the wall, and therefore, an overall improved performance is achieved.

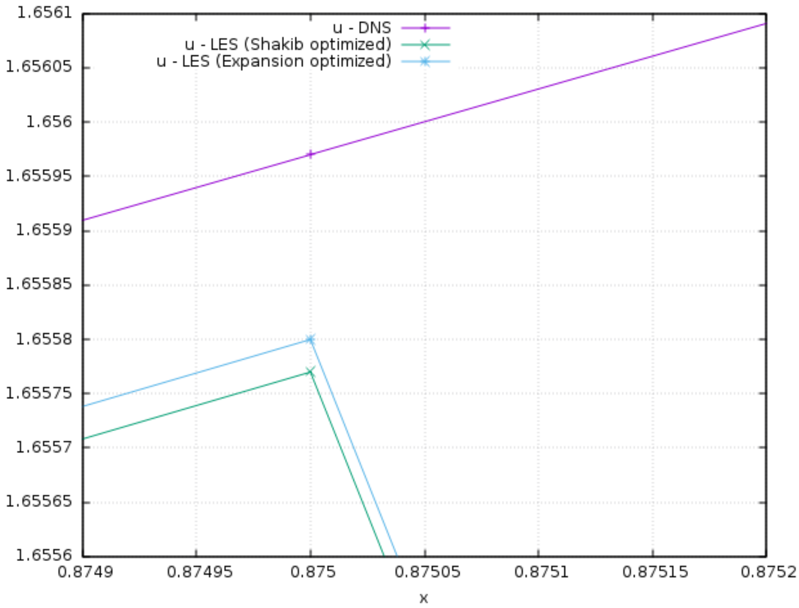

Figure 4.12: Comparison of stabilization methods for the near wall region $f = 1.0$.

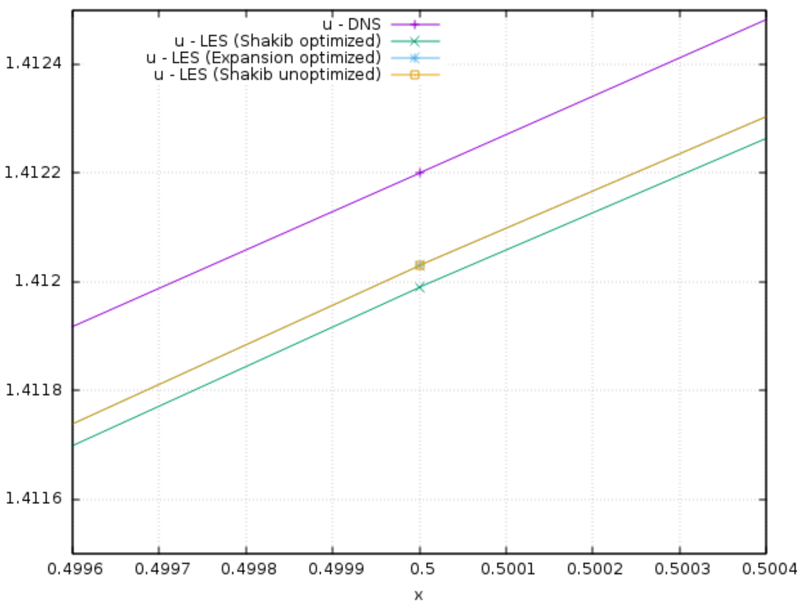

Figure 4.13: Comparison of stabilization methods for the mid-channel region $f = 1.0$.

Chapter 5

The Variational Multiscale Method applied to the Navier-Stokes equations

The necessity for three dimensions in turbulent flow stems essentially from the facts that in one dimension (Burgers) there is no chaotic response of the PDE to the initial conditions, and in two dimensions, the turbulent structures tend to merge, rather than break down to the energy dissipating scales, resulting in an inverse energy cascade. Additionally and more importantly, the truly useful applications of turbulent flow study for aerospace engineering will normally be found in the context of three dimensional problems. While the previously presented modeling approaches have been demonstrated as proofs of concept for the Burgers equation, it is now necessary to migrate them to the Navier-Stokes equations to show their real usefulness to aerospace applications. This chapter will attempt to demonstrate and extend some the previously treated approaches for a three dimensional case.

5.1 The weak formulation

Let us now begin from the incompressible form of the Navier-Stokes equations for Newtonian fluids; given in strong form by:

$$\frac{\partial \boldsymbol{u}}{\partial t} + \nabla \cdot (\boldsymbol{u} \otimes \boldsymbol{u}) + \nabla p - \nabla \cdot 2\nu \nabla^s \boldsymbol{u} = \boldsymbol{f} \tag{5.1}$$

$$\nabla \boldsymbol{u} = 0 \tag{5.2}$$

Where $\boldsymbol{u}$ represents the velocity vector $\boldsymbol{u} = [u \ v \ w]^T$, p stands for the pressure, and ν for the kinematic viscosity, which will be assumed constant and positive. Furthermore, $\nabla^s \boldsymbol{u}$ stands for the symmetric velocity gradient, which makes the momentum equation rotationally invariant, and $\otimes$ denotes the dyadic product, these two given as:

$$\nabla^s \boldsymbol{u} = \frac{1}{2}(\nabla \boldsymbol{u} + \nabla \boldsymbol{u}^T) \tag{5.3}$$

$$\boldsymbol{u} \otimes \boldsymbol{u} \equiv \boldsymbol{u}\ \boldsymbol{u}^T \tag{5.4}$$

Following a standard Galerkin method, just as detailed in subsection 2.1.2; the strong form of the NSE is multiplied by the test functions $\boldsymbol{w}$, q, and integrated over the domain. This allows defining the weak operators given by:

$$\begin{aligned} B(\boldsymbol{w}, q; \boldsymbol{u}, p) &= \left(\boldsymbol{w}, \frac{\partial \boldsymbol{u}}{\partial t}\right) - (\nabla \boldsymbol{w}, \boldsymbol{u} \otimes \boldsymbol{u}) + (q, \nabla \cdot \boldsymbol{u}) - (\nabla \cdot \boldsymbol{w}, p) + (\nabla^s \boldsymbol{w}, 2\nu \nabla^s \boldsymbol{u}) \\ F(\boldsymbol{w}, q) &= (\boldsymbol{w}, \boldsymbol{f}) \end{aligned} \tag{5.5}$$

Where $\boldsymbol{f}$ represents a source vector term. The trial solution, and testing function spaces are given by:

$$\boldsymbol{u} \in \quad \mathcal{S} \subset H^1(\Omega) \tag{5.6}$$

$$p \in \quad \mathcal{P} \subset L^2(\Omega) \tag{5.7}$$

$$\boldsymbol{w} \in \quad \mathcal{W} \subset H^1(\Omega) \tag{5.8}$$

$$q \in \quad \mathcal{Q} \subset L^2(\Omega) \tag{5.9}$$

With H^1, and L^2 once again defined as:

$$H^1 = \{h | h \in L^2, h_x \in L^2\} \tag{5.10}$$

$$L^2 = \{h | \int_\Omega (h)^2 d\Omega < \infty\} \tag{5.11}$$

Now, assuming the boundary conditions fulfill:

$$\boldsymbol{u} = 0 \quad \text{on } \Gamma \quad \forall \boldsymbol{u} \in \mathcal{S} \tag{5.12}$$

$$\boldsymbol{w} = 0 \quad \text{on } \Gamma \quad \forall \boldsymbol{w} \in \mathcal{W} \tag{5.13}$$

From where it is to be noted that a $\boldsymbol{u} = 0$ condition is only met for specific boundaries, as the test case description will later explain. And additionally assuming that the pressure has a zero mean condition given by:

$$\int_\Omega p\ d\Omega = 0 \quad \forall t \in]0, T[\tag{5.14}$$

The variational version of the NSE problem can be expressed as:

Find $\{\boldsymbol{u}, p\} \in [\mathcal{S}]^3 \times \mathcal{P}$ *such that* $\forall \{\boldsymbol{w}, q\} \in [\mathcal{W}]^3 \times \mathcal{Q}$*:*

$$B(\boldsymbol{w}, q; \boldsymbol{u}, p) = F(\boldsymbol{w}, q) \tag{5.15}$$

5.2 Weak boundary conditions

In Navier-Stokes problems it has been observed that strongly imposed no-slip conditions in the walls for insufficiently fine near-wall meshes leads to inaccurate mean velocity solutions [Bazilevs et al. (2007b)]. With sharp boundary layers present, it can be advantageous to treat Dirichlet boundary conditions weakly. This allows for improved coarse-mesh solution interpolations, as well as the possibility of introducing wall-stress models for LES/RANS as shown by Hulshoff et al. (2011). In the present context, it invokes the addition of a jump-term and an adjoint consistency term while relaxing the assumption that $w = 0$ on Γ. As pointed out by Bazilevs et al. (2007b), in the limit of vanishing mesh size in wall-normal direction, this formulation acts like a strong Dirichlet boundary condition. Given the level of refinement and structure of the employed mesh (which will be later explained), the use of the formulation by Hulshoff et al. (2011) aided in the improvement of the results over the use of strongly imposed Dirichlet B.Cs. and will hereafter be referred to as the **g - method**.

5.3 The Variational Multiscale problem

Once again, up to this point only a Variational formulation of the NSE has been derived. A Multiscale problem requires the decomposition of quantities into different scales. For this, the trial solutions and test functions in the NSE will be split into large and small scales, such that:

$$\boldsymbol{u} = \overline{\boldsymbol{u}} + \boldsymbol{u'} \tag{5.16}$$
$$p = \overline{p} + p' \tag{5.17}$$
$$\boldsymbol{w} = \overline{\boldsymbol{w}} + \boldsymbol{w'} \tag{5.18}$$
$$q = \overline{q} + q' \tag{5.19}$$

Where $\bar{\cdot}$, and $\cdot'$ represent the large and small scales respectively. The trial solution and testing function spaces are now accordingly separated as:

$$\begin{aligned}
\mathcal{S} &= \overline{\mathcal{S}} \oplus \mathcal{S}' \\
\mathcal{P} &= \overline{\mathcal{P}} \oplus \mathcal{P}' \\
\mathcal{W} &= \overline{\mathcal{W}} \oplus \mathcal{W}' \\
\mathcal{Q} &= \overline{\mathcal{Q}} \oplus \mathcal{Q}'
\end{aligned}$$

Now employing (5.16) through (5.19), the large-scales equation is given as:

$$\begin{aligned}
&\left(\overline{\boldsymbol{w}}, \frac{\partial \overline{\boldsymbol{u}}}{\partial t}\right) - (\nabla \overline{\boldsymbol{w}}, \overline{\boldsymbol{u}} \otimes \overline{\boldsymbol{u}}) + (\overline{q}, \nabla \cdot \overline{\boldsymbol{u}}) - (\nabla \cdot \overline{\boldsymbol{w}}, \overline{p}) + (\nabla^s \overline{\boldsymbol{w}}, 2\nu \nabla^s \overline{\boldsymbol{u}}) \\
&+ \left(\overline{\boldsymbol{w}}, \frac{\partial \boldsymbol{u'}}{\partial t}\right) - (\nabla \overline{\boldsymbol{w}}, \boldsymbol{u'} \otimes \boldsymbol{u'}) + (\overline{q}, \nabla \cdot \boldsymbol{u'}) - (\nabla \cdot \overline{\boldsymbol{w}}, p') + (\nabla^s \overline{\boldsymbol{w}}, 2\nu \nabla^s \boldsymbol{u'}) \\
&\qquad - (\nabla \overline{\boldsymbol{w}}, \overline{\boldsymbol{u}} \otimes \boldsymbol{u'}) - (\nabla \overline{\boldsymbol{w}}, \boldsymbol{u'} \otimes \overline{\boldsymbol{u}}) = (\overline{\boldsymbol{w}}, \boldsymbol{f})
\end{aligned} \tag{5.20}$$

Where once again, the assumption of quasi-steady small-scales allows neglecting the $\left(\overline{\boldsymbol{w}}, \frac{\partial \boldsymbol{u'}}{\partial t}\right)$ term. The large scales variational problem can therefore be expressed as:

Find $\{\overline{\boldsymbol{u}}, \overline{p}\} \in [\overline{\mathcal{S}}]^3 \times \overline{\mathcal{P}}$ *such that* $\forall \{\overline{\boldsymbol{w}}, \overline{q}\} \in [\overline{\mathcal{W}}]^3 \times \overline{\mathcal{Q}}$*:*

$$B(\overline{\boldsymbol{w}}, \overline{q}; \overline{\boldsymbol{u}} + \boldsymbol{u'}, \overline{p} + p') = F(\overline{\boldsymbol{w}}, \overline{q}) \tag{5.21}$$

5.4 Modeling the small scales

Following the logic of section 3.1.2, the effects of the unresolved scales $\{\boldsymbol{u'}, p'\}$ in (5.21) can be approximated through a stabilization term which now for the 3D case of the NSE, takes the form of a vector which reads:

$$\boldsymbol{u'} \approx -\boldsymbol{\tau}\boldsymbol{\mathcal{R}} \tag{5.22}$$

Where now $\boldsymbol{\mathcal{R}}$ is the residual of the large scales as given by:

$$\boldsymbol{\mathcal{R}} = \begin{bmatrix} \boldsymbol{r}_M(\overline{\boldsymbol{u}}, \overline{p}) \\ r_C(\overline{\boldsymbol{u}}) \end{bmatrix} \tag{5.23}$$

Same which has its components computed from the strong form of the momentum and continuity equations, and given by:

$$\boldsymbol{r}_M(\overline{\boldsymbol{u}}, \overline{p}) = \frac{\partial \overline{\boldsymbol{u}}}{\partial t} + \overline{\boldsymbol{u}} \cdot \nabla \overline{\boldsymbol{u}} + \nabla p - \nu \Delta \overline{\boldsymbol{u}} - \boldsymbol{f} \tag{5.24}$$

$$r_c(\overline{\boldsymbol{u}}) = \nabla \overline{\boldsymbol{u}} \tag{5.25}$$

Additionally, the formulation of $\boldsymbol{\tau}$ is chosen to be a diagonal 4×4 matrix which is a nonlinear extension of the classical stabilization for the incompressible NSE [Franca and Frey (1992)] and given as:

$$\boldsymbol{\tau} = \begin{bmatrix} \tau_M & 0 & 0 & 0 \\ 0 & \tau_M & 0 & 0 \\ 0 & 0 & \tau_M & 0 \\ 0 & 0 & 0 & \tau_C \end{bmatrix} \tag{5.26}$$

Following the process detailed in Akkerman (2009), a reconstruction for the unresolved scales can be started from the Euler-Langrange equations of the small-scales part of the problem, given by:

$$\frac{\partial \boldsymbol{u'}}{\partial t} + \nabla(\overline{\boldsymbol{u}} \otimes \boldsymbol{u'} + \boldsymbol{u'} \otimes \overline{\boldsymbol{u}} + \boldsymbol{u'} \otimes \boldsymbol{u'}) + \nabla p' - \nabla^s 2\nu \nabla^s \boldsymbol{u'} = -\boldsymbol{r}_M(\overline{\boldsymbol{u}}, \overline{p}) \tag{5.27}$$

$$\nabla \boldsymbol{u'} = -r_c(\overline{\boldsymbol{u}}) \tag{5.28}$$

Now, employing a discrete approximation of the gradient/divergence operator denoted by $\boldsymbol{g}$; and a 3×3 matrix τ_M^{-1} to represent algebraic approximations for the differential operators, (5.27), and (5.28) can be expressed as:

$$\tau_M^{-1}\boldsymbol{u'} - \boldsymbol{g}p' = -\boldsymbol{r}_M(\overline{\boldsymbol{u}}, \overline{p}) \tag{5.29}$$

$$\boldsymbol{g} \cdot \boldsymbol{u'} = -r_c(\overline{\boldsymbol{u}}) \tag{5.30}$$

Multiplying the approximation of the small-scales momentum equation (5.29) by $\boldsymbol{g} \cdot \tau_M$ gives:

$$\boldsymbol{g} \cdot \boldsymbol{u'} - \boldsymbol{g} \cdot \tau_M \boldsymbol{g} p' = -\boldsymbol{g} \cdot \tau_M \boldsymbol{r}_M(\overline{\boldsymbol{u}}, \overline{p}) \tag{5.31}$$

Where the substitution of (5.30) yields:

$$\boldsymbol{g} \cdot \tau_M \boldsymbol{g} p' = \boldsymbol{g} \cdot \tau_M \boldsymbol{r}_M(\overline{\boldsymbol{u}}, \overline{p}) - r_C(\overline{\boldsymbol{u}}) \tag{5.32}$$

By neglecting $\tau_M \boldsymbol{r}_M(\overline{\boldsymbol{u}}, \overline{p})$, it is possible to arrive to a diagonal $\boldsymbol{\tau}$, resulting in:

$$p' = -(\boldsymbol{g} \cdot \tau_M \boldsymbol{g})^{-1} r_c(\overline{\boldsymbol{u}}) \tag{5.33}$$

Yielding finally an expression for τ_C given by:

$$\tau_C = -(\boldsymbol{g} \cdot \tau_M \boldsymbol{g})^{-1} \tag{5.34}$$

With these descriptions of $\boldsymbol{\tau}$, and $\boldsymbol{\mathcal{R}}$, once again the quality of the estimation of the unresolved scales effects relies in the form given to $\boldsymbol{\tau}$, or more specifically, to τ_M. Previous research has defined some formulations for this term, for example, following the theory of of stabilized methods for linear advection-diffusion systems as in Hughes and Mallet (1986), and Shakib et al. (1991), a definition for τ_M can be:

$$\tau_M = \left[\frac{4}{\Delta t^2} + \overline{\boldsymbol{u}} \cdot \boldsymbol{G} \overline{\boldsymbol{u}} + 3\nu^2 \boldsymbol{G} : \boldsymbol{G} \right]^{-1/2} \tag{5.35}$$

Where $\cdot : \cdot$ stands for the double contraction.

For the case of the Burgers equations, the optimizations to the models were made from DNS data. Provided that the test case for the NSE (channel flow) has been extensively studied, DNS data is also available and will be employed for the computations. However, it is worth once again pointing out that the intention of this research is to explore the feasibility of coupling RANS and LES methods through the SGS model. Having said this, the expected reference data for future applications of this method would normally not come from time-averaged DNS, but instead from less expensive RANS runs. The following chapters will describe the formulations and results of the method applied to the NSE.

Chapter 6

Channel flow test case and baseline coarse mesh results

In this chapter, a brief inspection of the baseline SGS models will be presented. The intention of this is to obtain benchmark performance data as a reference for the evaluation of the proposed improvements. A description of the test case will be provided now, followed by the initial results.

6.1 Description of the test cases

Based on the work of Kim et al. (1987) and later Moser et al. (1999), the use of a turbulent channel flow allows for the demonstration of the existing SGS models, and provides a "simple" framework for improvements and testing. Regarding the spanwise and streamwise directions, a particular choice of boundary conditions is made in order to ease the computations and measurements. While say for example a uniform inlet in a wall bounded channel would require enough spatial and temporal lengths for the turbulent structures to fully develop; the use of periodic B.Cs. allows for reduced computation domains. By feeding the information from one boundary to its opposite as shown in figure 6.1, the turbulent structures are homogeneous in said directions, limiting the wall-bounded characteristics to the normal direction. The boundary layer will develop only in such direction, and given the symmetry of the case, a half-channel observation will allow drawing conclusions from the computed data. Additionally, the channel dimensions are chosen such that "the two-point correlations in streamwise and spanwise directions would be essentially zero at maximum separation".

As observed by Moser et al. (1999), the initial work of Kim et al. (1987) employed a $Re_\tau = 180$, for which the existence of a log layer might be questionable. However, as explained later, this cases are still of interest for the purposes here pursued. Additionally, some initial conditions and reference statistics are obtained from DNS runs by Hoyas and Jiménez (2008), del Álamo

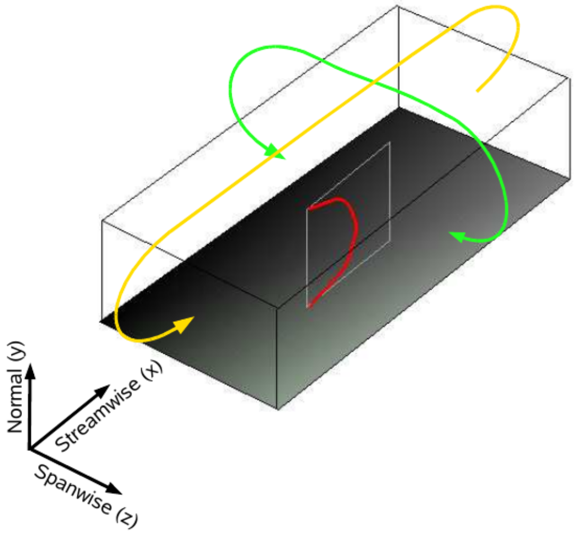

Figure 6.1: Boundary conditions in channel flow

and Jiménez (2003). While Moser et al. (1999) employed a dynamic pressure gradient to maintain a constant mass flow, the tests for this work used a uniform forcing term given by the vector:

$$\boldsymbol{f} = \begin{bmatrix} 1.0 \\ 0.0 \\ 0.0 \end{bmatrix} \tag{6.1}$$

to drive the channel. A stabilization parameter as given by (5.35) based on the work of Bazilevs et al. (2007a) will serve as a benchmark or start point, just as Shakib's τ employed for the previously described Burgers stabilization.

6.1.1 The reference spectra

From the data provided by Moser et al. (1999), the spectra for $Re_\tau = 180$ is plotted and shown in figure 6.2. Although turbulent, this case is not optimum in that it contains low-Re effects and no substantial inertial range. It is however effective for preliminary studies as its mesh refinement requirements are low. The location of the start of the inertial range is ambiguous in this case, but based on the spacing reported by Moser et al. (1999), meshes of at least 16^3 to 24^3 elements are required to resolve part of the inertial range.

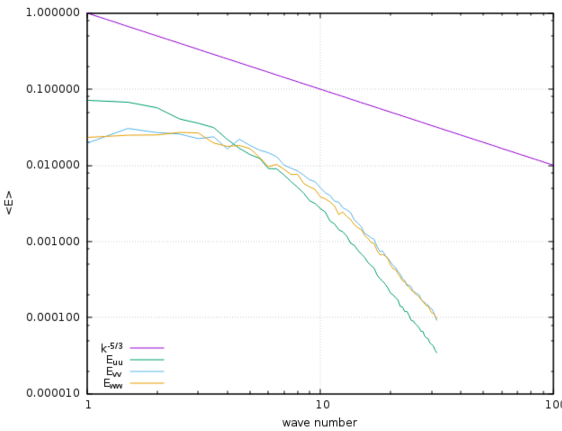

(a) x spectra

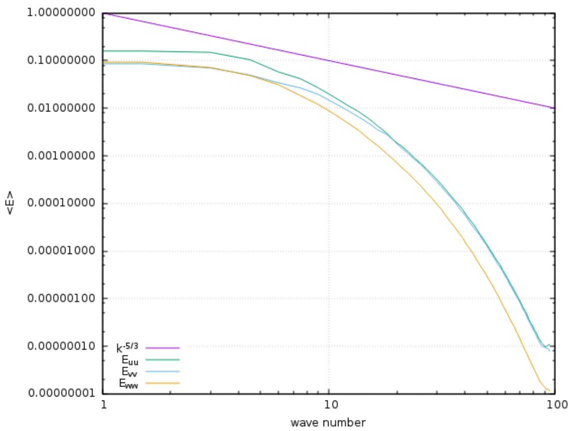

(b) z spectra

Figure 6.2: Spectra for $Re_\tau = 180$ channel flow by Moser et al. (1999)

6.2 Initial Runs

The initial runs set a benchmark for the improvement which will be obtained by optimizing the SGS models. Based on the previously mentioned reference data, a solution projection of DNS resolution is made unto the desired LES mesh, which initializes the fluctuations in the flow field for the appropriate modes to be further driven by $\boldsymbol{f}$.

6.2.1 The 8^3 grid

We begin by considering a very coarse case of 8^3 elements, where the resolution is insufficient for resolving any of the inertial range. At such low resolutions, approximations like (5.35) cannot be expected to provide realistic results. However, such resolutions are interesting for examining the control authority of the model in regions for which the only goal is to match mean flow statistics. With this in mind, the first test cases are made in this $8 \times 8 \times 8$ grid, where the test parameters are defined as:

$$Re_\tau = 180, \quad \Delta t = 6.25 \times 10^{-3} s, \quad T = 300s, \quad N_{x,y,z} = [8\ 8\ 8]$$

Figure 6.3 shows the bulk velocity measurements with respect to time for this test case. While the reference data indicates a bulk velocity of uBulk $= 15.68\ m/s$, and furthermore, the test case is initialized to such data, an initial transient state can be seen. The steady state conditions for the collection of data and thus for the computation of flow statistics are considered to start at $t = 100s$, which as can be seen in again in figure 6.3 is a suitable point in time to consider the transient phenomena as faded. This transient state derives from the fact that the new mesh (LES grid) reduces the accuracy of the computations, and evidently a considerable amount of data is lost in the projection of the initial conditions.

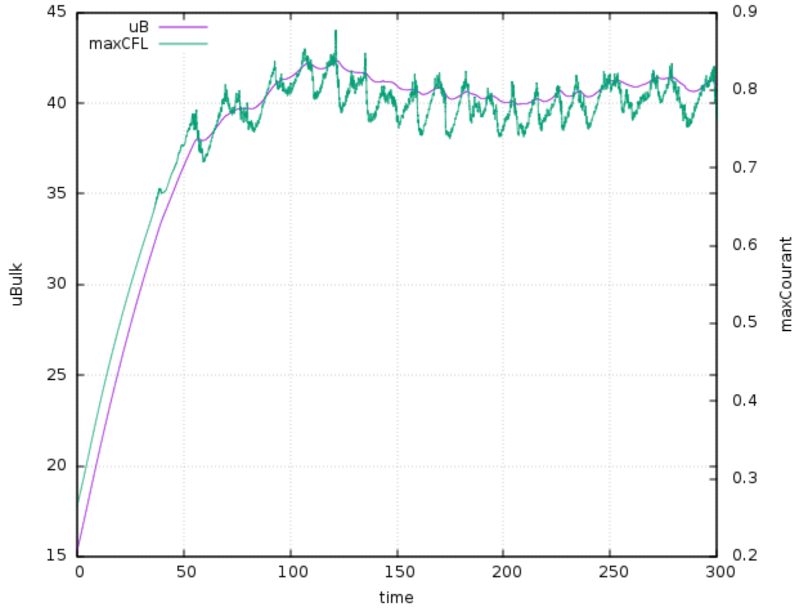

Figure 6.3: Bulk velocity for benchmark channel flow

From here that the statistics of the baseline flow predictably exhibit a mismatch with the reference data. Similarly to the Burgers cases, the base stabilization term as given by (5.26) with τ_M as given by (5.35), and hereafter denoted $\boldsymbol{\tau_{Baz}}$; is enough to allow the convergence of the numerical method, and to some extent, provide an approximation of the small scales. The shortcomings of this formulation become evident in the mismatches between the LES solutions and the DNS reference profiles as shown in figure 6.4.

For purposes which will later be explained, graphs of τ_M and τ_C are shown in figure 6.5. Note should be taken on the fairly uniform distribution of both parameters in the wall normal direction. Such behavior stems from the magnitude of the terms in the τ_M formulation as given by (5.35). Denoting the terms in τ_M as:

$$A = \frac{4}{\Delta t^2} \tag{6.2}$$

$$B = \overline{\boldsymbol{u}} \cdot \boldsymbol{G}\overline{\boldsymbol{u}} \tag{6.3}$$

$$C = 3\nu^2 \boldsymbol{G} : \boldsymbol{G} \tag{6.4}$$

Plots of their magnitude throughout the domain can be made, same which are shown in figure 6.6. As it can be seen, the magnitude of A is is considerably higher that that of B, and several orders of magnitude above C. The distribution of $\boldsymbol{\tau_{Baz}}$ as shown in figure 6.5 can therefore be thought of as dominated by A, which is an important observation for the coming work.

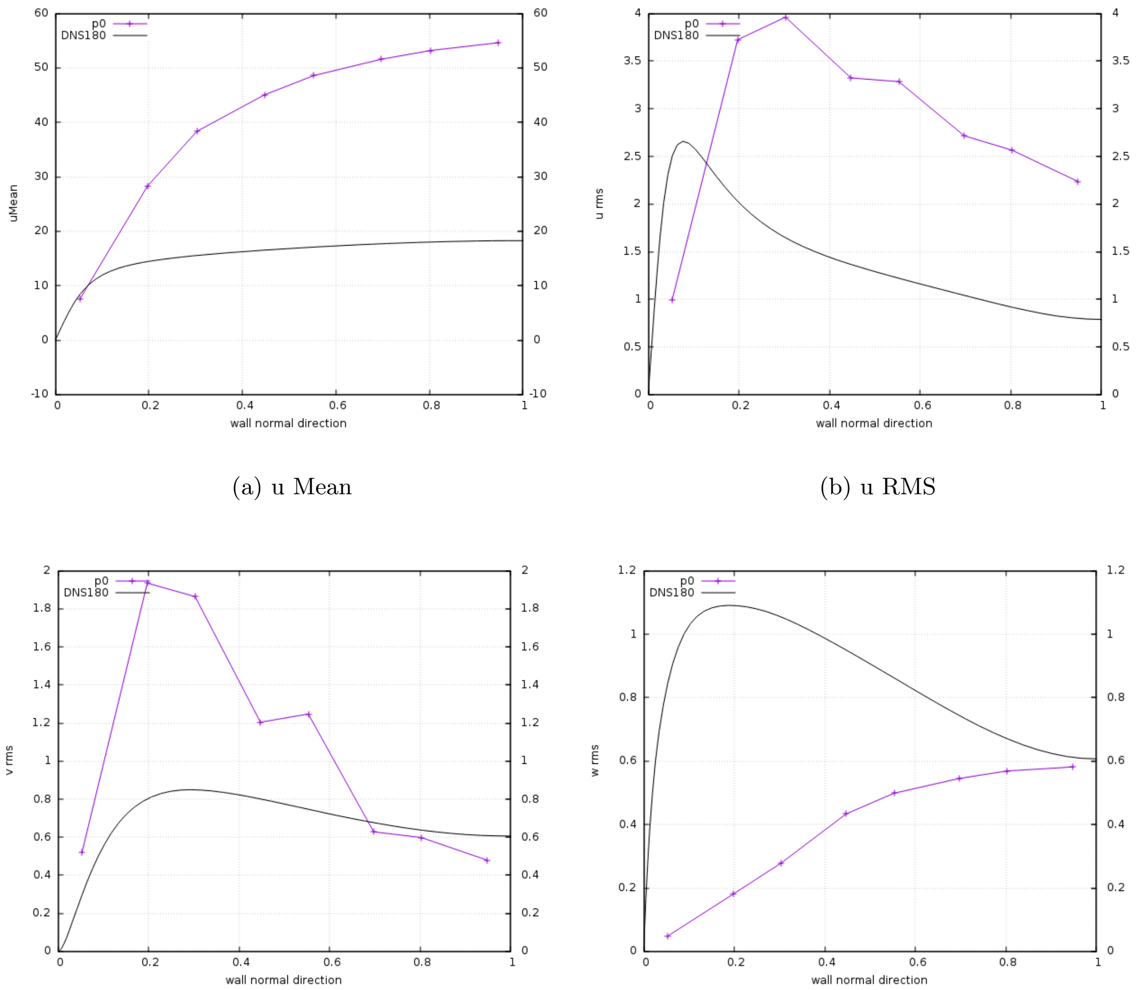

(a) u Mean

(b) u RMS

(c) v RMS

(d) w RMS

Figure 6.4: Statistics profiles for initial NSE runs

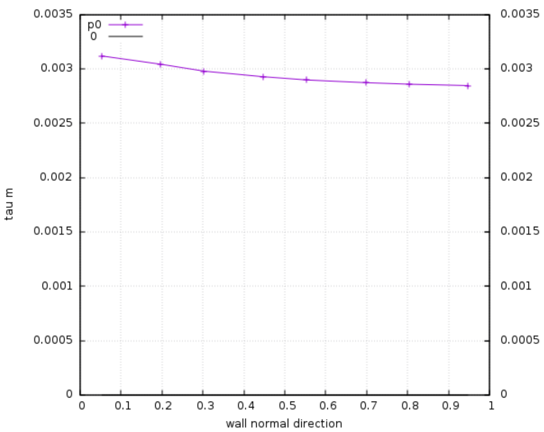

(a) τ_M

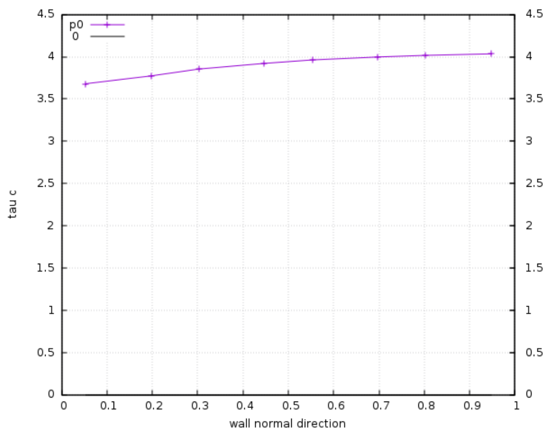

(b) τ_C

Figure 6.5: τ_M and τ_C distriburtion for initial NSE runs

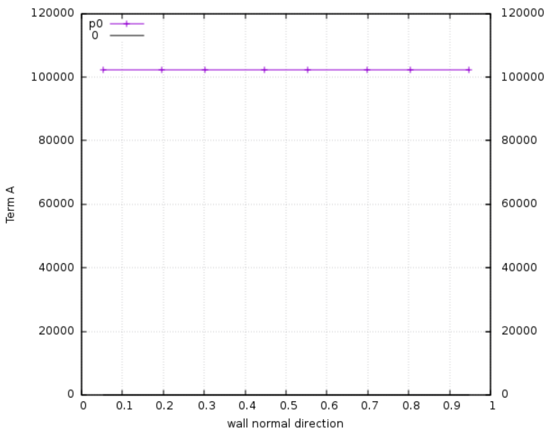

(a) Term A

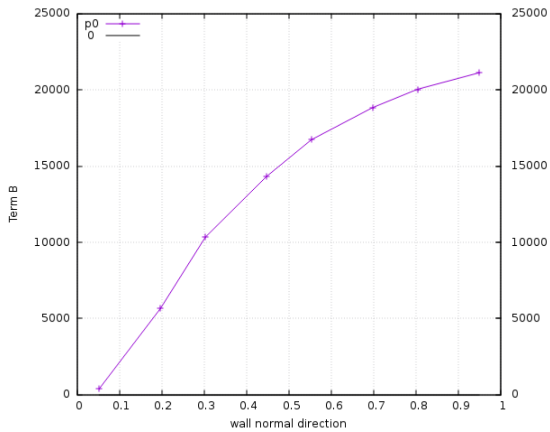

(b) Term B

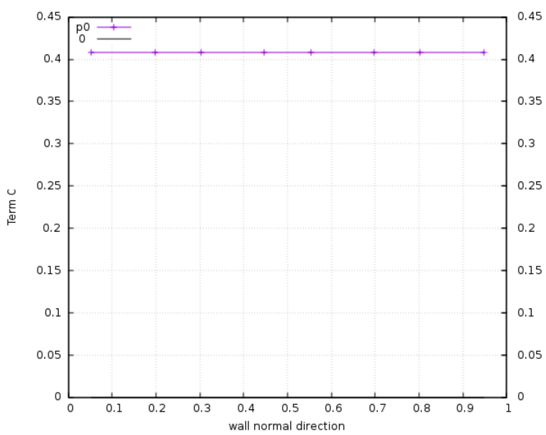

(c) Term C

Figure 6.6: Distribution of the τ_M components in wall normal direction

6.2.2 Increased spatial refinement

Providing realistic boundary conditions for the full LES regions requires resolving more physics than can be represented with an 8^3 mesh. With this in mind, runs were made in refined meshes of 16^3, 32^3 and 48^3 elements. A comparison of results with the baseline case is shown in figure 6.7, for which the expected trends are followed, exhibiting increased accuracy with reduced grid spacing.

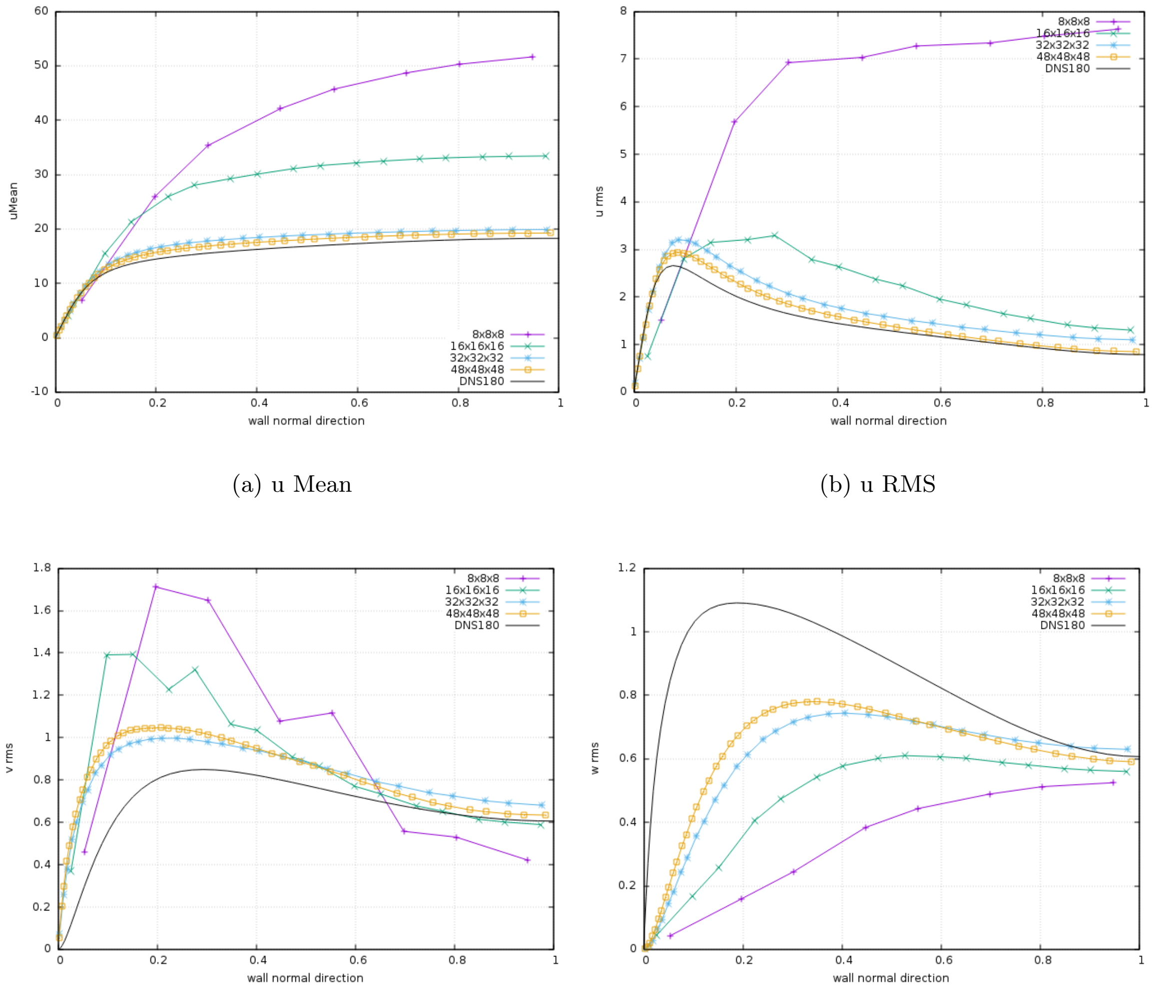

(a) u Mean

(b) u RMS

(c) v RMS

(d) w RMS

Figure 6.7: Statistics profiles for grid refinement runs

6.2.3 Weakly imposed boundary conditions

The final set of benchmark runs involves a comparison of the boundary conditions enforcement method. As discussed in section 5.2, it is possible to obtain closer matches of the mean profiles by relaxing the no-slip conditions at the walls. A comparison of the B.Cs. enforcement was therefore made for a 16^3 mesh. The results shown in figures 6.8, evidence that the g-method provides improved results when matching the means, while creating only minor deviations in the fluctuations profiles. When using VMM models on coarse meshes, it appears negative velocities are required to achieve a realistic energy balance. This does not occur when eddy viscosity models are used as shown in Hulshoff et al. (2011).

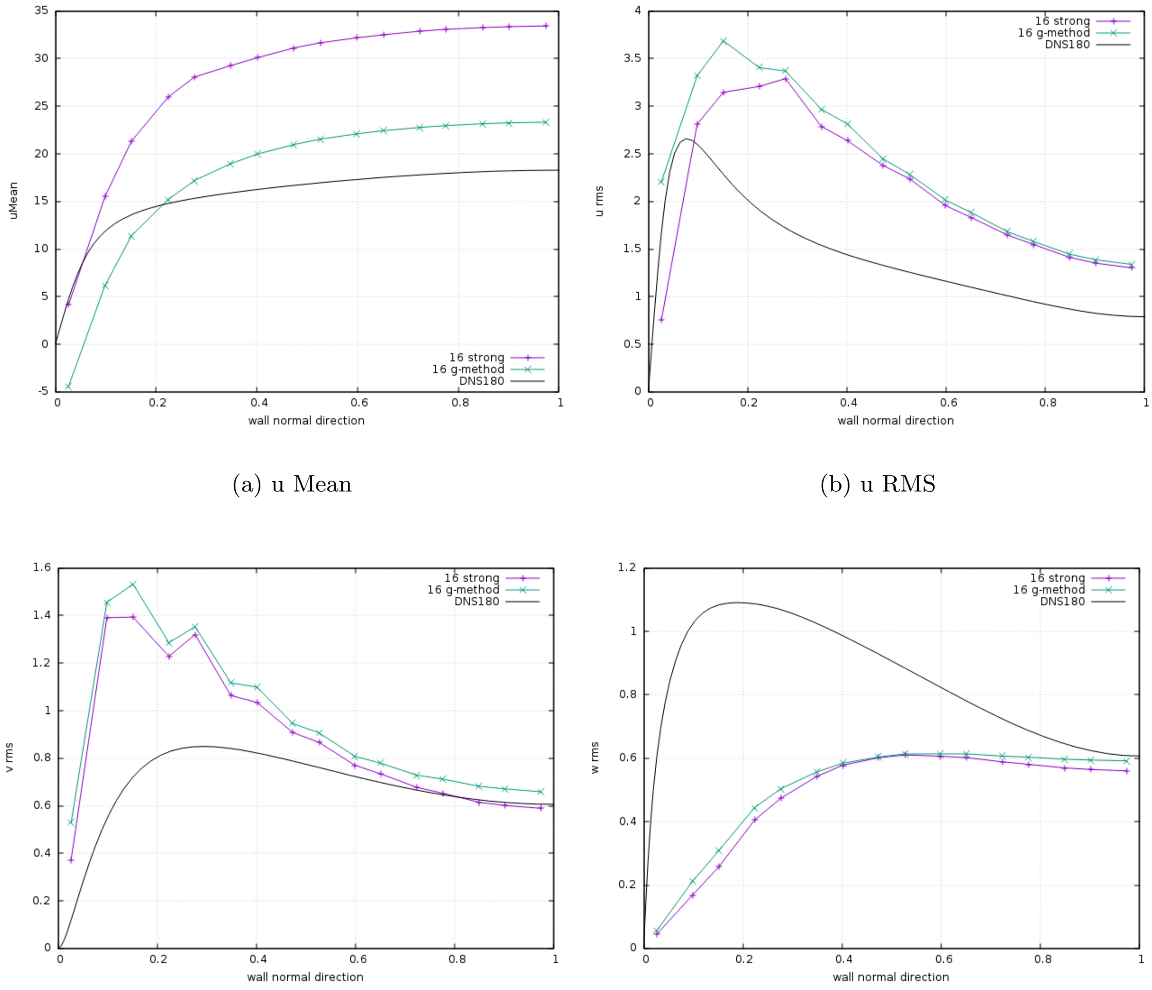

(a) u Mean

(b) u RMS

(c) v RMS

(d) w RMS

Figure 6.8: Statistics profiles for different enforcements of boundary conditions $Re_\tau = 180$

Having established the baseline behavior under different conditions, the optimization methods and runs are discussed in the following chapter.

Chapter 7

Improvements to SGS models

Following an adapted, however in essence similar logic to that in sections 4.1, and 4.2, modified formulations for $\boldsymbol{\tau_{Baz}}$ and expanded approximations for $\boldsymbol{u'}$ were elaborated and tested to improve the LES results. Once again, these optimizations are driven by reference data, and while the methodology remains fundamentally equivalent to the previously used, the computations are predictably more complex. While the training norm introduced in 4.1.2 proved effective and inexpensive in the context of Burgers, it is replaced here by a more expensive method, given the unsteady and three dimensional nature of these computations. This will therefore limit the exploratory capabilities of the optimizations, however these still prove able to return useful data.

7.1 Green's function optimization

Migrating the ideas demonstrated for the Burgers equation in section 4.1, an attempt of improvement is made by a modification of the local Green's function employed to model the small-scales. For this SGS model, the inclusion of free coefficients as described by:

$$\tau_M = \left[\gamma_0 \ \frac{1}{\Delta t^2} + \gamma_1 \ \overline{\boldsymbol{u}} \cdot \boldsymbol{G} \overline{\boldsymbol{u}} + \gamma_2 \ \nu^2 \boldsymbol{G} : \boldsymbol{G} \right]^{-1/2} \tag{7.1}$$

will serve a starting point to the optimizations. The free coefficients $\gamma_{0,1,2}$ will provide some control to $\boldsymbol{\tau_{Baz}}$ such that an improvement on the baseline results can be made. The error in the bulk velocity for a $Re_\tau = 180$ case, is given by:

$$\epsilon_{uBulk} = \frac{1}{N_T} \sum_{i=0}^{N_T} |u\mathrm{Bulk}_i - 15.68| \tag{7.2}$$

Where N_T represents the total number of time steps. Alternatively, the error in the mean velocity profile, is given by:

$$\epsilon_{uMean} = \frac{1}{N_T} \sum_{i=0}^{N_T} \sqrt{\sum_{j=0}^{N_X} \Delta \ u\mathrm{Mean}_j} \tag{7.3}$$

$$\Delta \ u\mathrm{Mean}_j = u\mathrm{Mean}_{LES_j} - u\mathrm{Mean}_{DNS_j} \tag{7.4}$$

These definitions will be used forth to construct the response surfaces and henceforth referred to as the **simulation norms**.

7.1.1 Initial sweep

As mentioned in section 6.2.1, on an 8^3 mesh at $Re_\tau = 180$ it is not expected that an SGS model based on linearized theory will be capable of reproducing the small scales very accurately. It is interesting however to explore which is the overall control effect on coarse meshes where u' is large, with the current objective of matching the statistics rather than a detailed turbulence analysis. With this in mind, the optimization runs were made employing the same parameters defined for the baseline case and given as:

$$Re_\tau = 180, \quad \Delta t = 6.25 \times 10^{-3} s, \quad T = 300s$$

A simulation norms evaluation was made for $\gamma_1 = [1\ 2\ 3\ 4\ 5]$, and $\gamma_2 = [3\ 20\ 36\ 52\ 69]$, while maintaining an unmodified $\gamma_0 = 4.0$. From here to be noted that the test matrix has only 25 combinations, unlike the 40,000 values for the Burgers tests, evidencing the previously mentioned cost issue. As said before, this derives from the fact that this error calculations are done by comparing LES solutions to the DNS reference data, and not from a weak form residual; therefore, requiring a full LES simulation for each coefficient combination. The reason for which a training norm cannot be used in this context is that the reference data is not a full space-time data set, instead only the statistics are available. Figure 7.1 shows the response surfaces for the errors as obtained through (7.2), and (7.3).

A minimum point is now obtained from the response surfaces, which is common for both error measurements and located at $\gamma_1 = 1.0$, $\gamma_2 = 52.0$. A comparison of the “optimized” and standard profiles can now be made, and is shown in figure 7.2. Except for the fluctuations in u, the profiles can be seen to have very slight changes after the error minimization study.

As shown in figure 7.4, despite the 5-fold change in γ_1, and higher than an order of magnitude shift in γ_2, the $\boldsymbol{\tau_{Baz}}$ distribution and magnitudes are barely affected, confirming the observations indicated in the previous chapter. While a large variation in γ_2 produces a large shifting in term C as shown in figure 7.5, it can barely generate a change in the profiles, given its relative magnitude. This can be better visualized by a surface plot of the response surfaces in figure 7.3, which shows that the variations in the simulation norm are not significant with respect to changes in $\gamma_{1,2}$. Having these observations, a second test is made, now for a $\gamma_{0,1}$ sweep, which will allow to increase the effectiveness of modifications to terms A and B, while analyzing the response to an invariant term C.

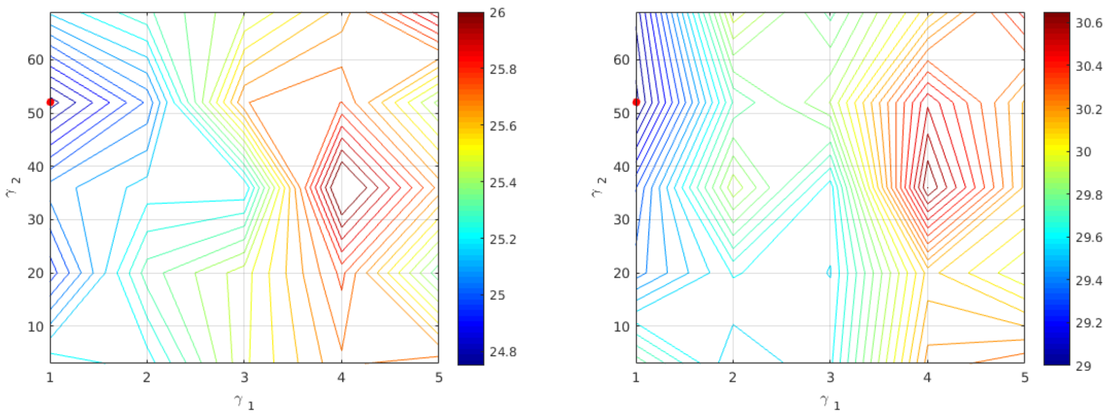

(a) u Bulk

(b) u Mean

Figure 7.1: Response surfaces for optimization runs

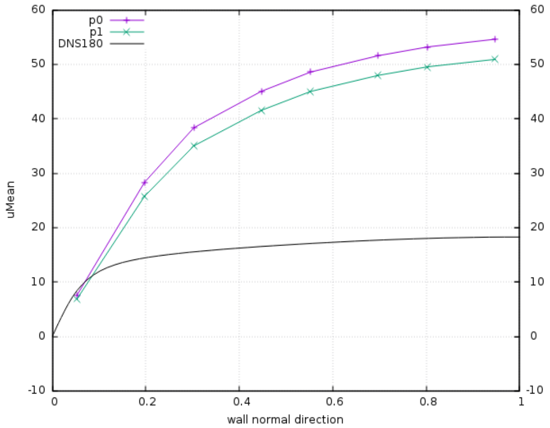

(a) u Mean

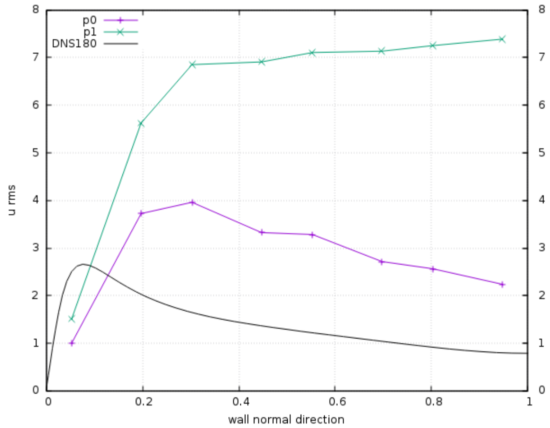

(b) u RMS

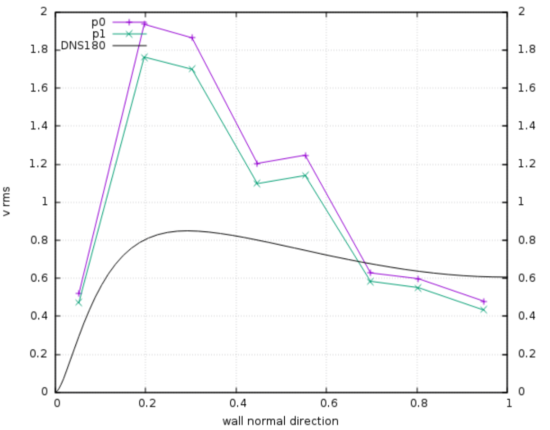

(c) v RMS

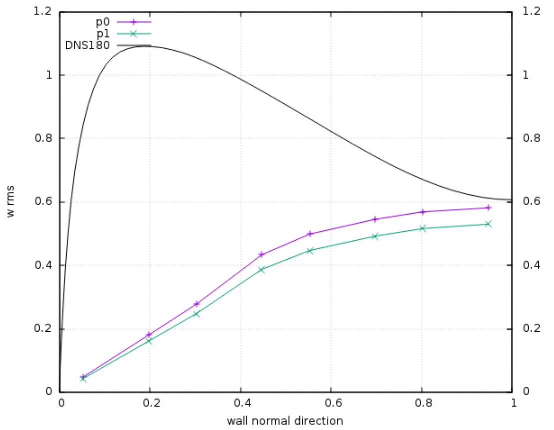

(d) w RMS

Figure 7.2: Statistics profiles for initial optimization runs

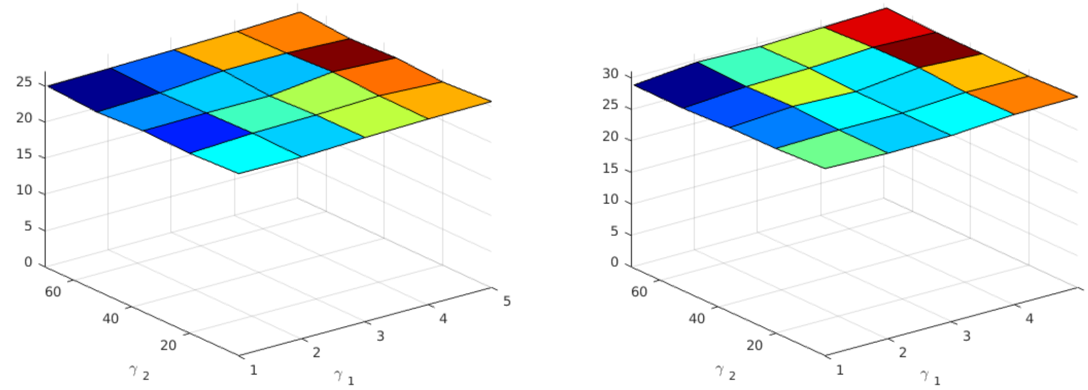

(a) u Bulk (b) u Mean

Figure 7.3: Alternate representation of the response surfaces for optimization runs

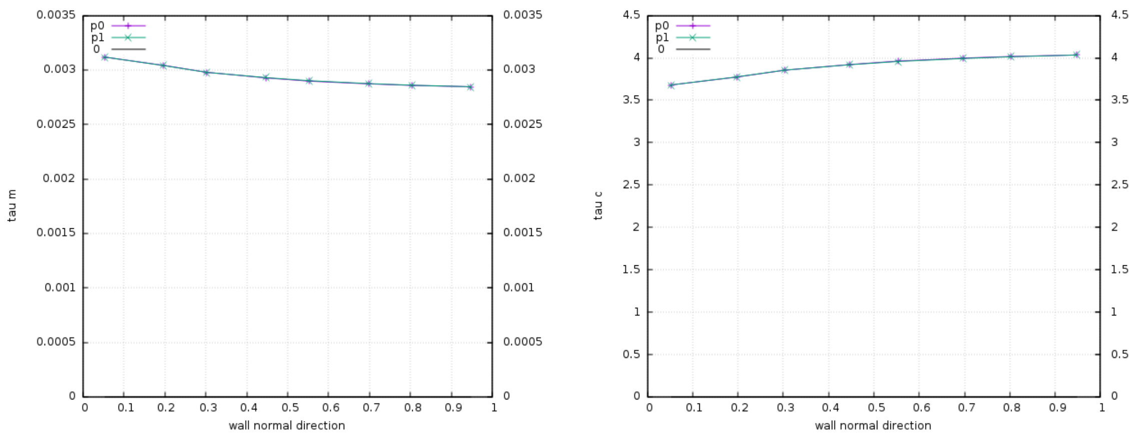

(a) τ_M (b) τ_C

Figure 7.4: τ_M and τ_C distribution for initial optimizations

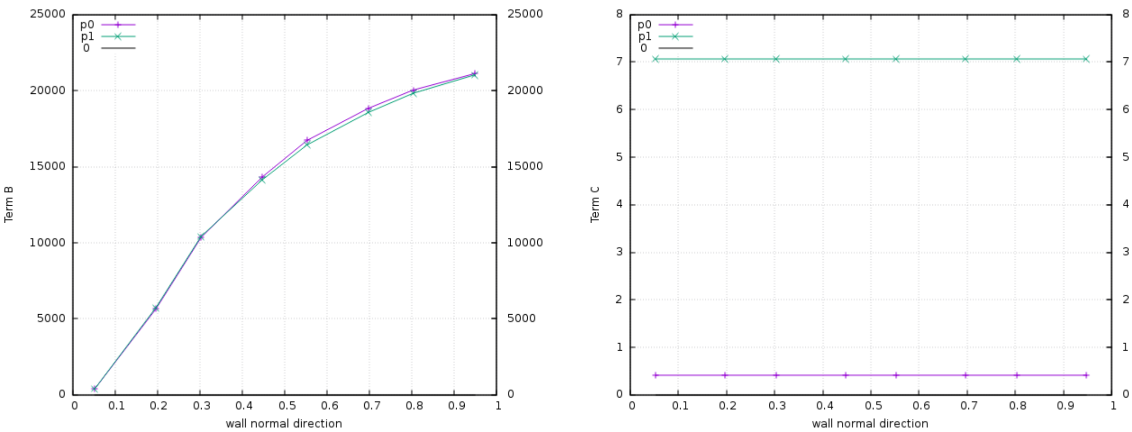

(a) Term B

(b) Term C

Figure 7.5: Distribution of the τ_M components in wall normal direction

7.1.2 Adapting the unsteady term

An adaptation of the unsteady term A aims to understand its dominance in the formulation, for this, a new sweep was made for $\gamma_{0,1}$, leaving a fixed $\gamma_2 = 3.0$. This is done with the objective of improving the authority over the response, and thus, obtain closer matches in the profiles. Figure 7.6, displays the response surfaces of a sweep performed for $\gamma_0 = [0.01\ 0.05\ 0.1\ 0.5\ 1\ 2]$, and $\gamma_1 = [0.1\ 1\ 5\ 10\ 20\ 100]$. It can clearly be seen that the response amplitude has increased for a less dominant term A.

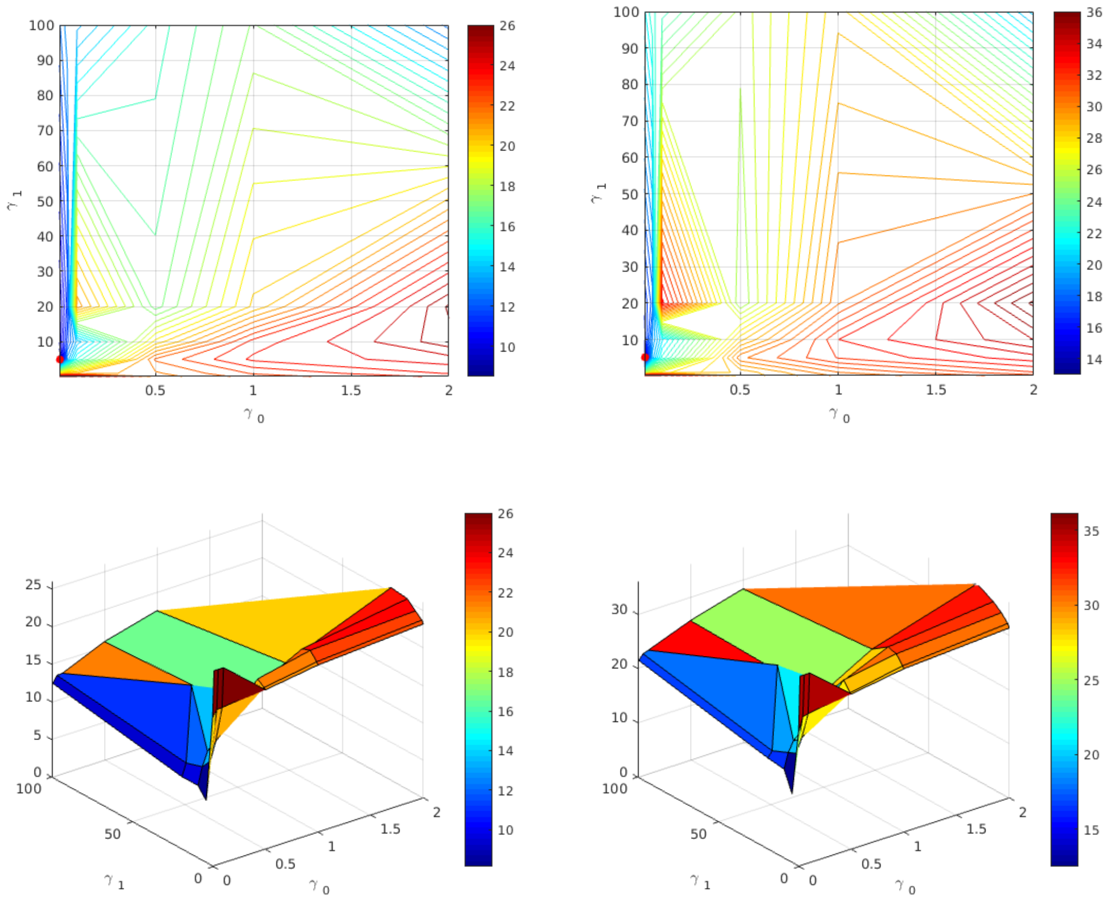

(c) u Bulk

(d) u Mean

Figure 7.6: Response surfaces for optimization runs

A following run under the optimized coefficients yields set of improved profiles, same which is displayed in figure 7.7. It is evidenced here that the control exerted on the formulation has increased by reducing the influence of its time dependent parameter. While a closer match of the mean velocities and v fluctuations is obtained, a disagreement of this behavior is seen in the u and w fluctuation profiles, a trend which will later be elaborated on.

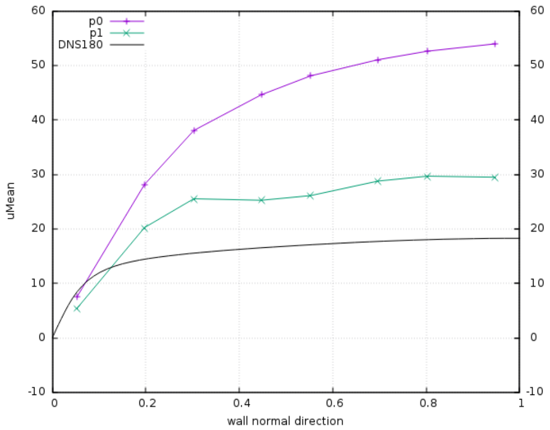

(a) u Mean

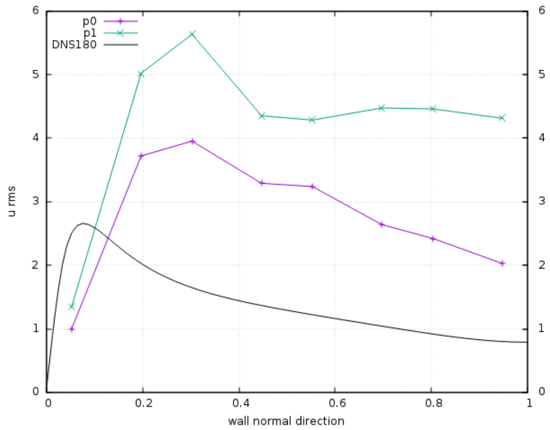

(b) u RMS

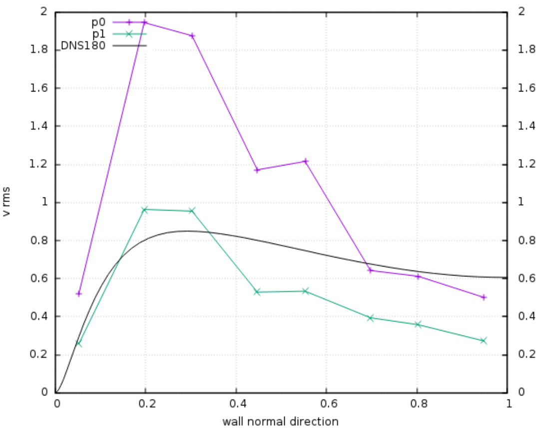

(c) v RMS

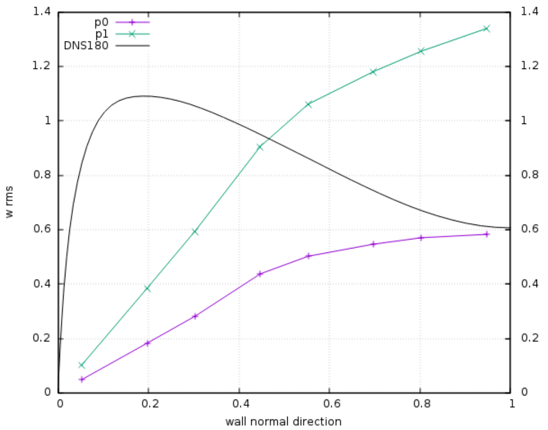

(d) w RMS

Figure 7.7: Statistics profiles for initial optimization runs. p0, baseline run (purple); p1, optimized run (green)

It can additionally be seen from figure 7.8 that the $\boldsymbol{\tau_{Baz}}$ distribution has been localized given the reduced influence of the constant and previously dominating term A. This is further verified by figure 7.9, which not only evidences drastic reduction of term A, but now also a more responsive term B. For this purposes, term C is not shown given that as discussed before, its influence is negligible, and in this test case invariant between the baseline and optimized cases.

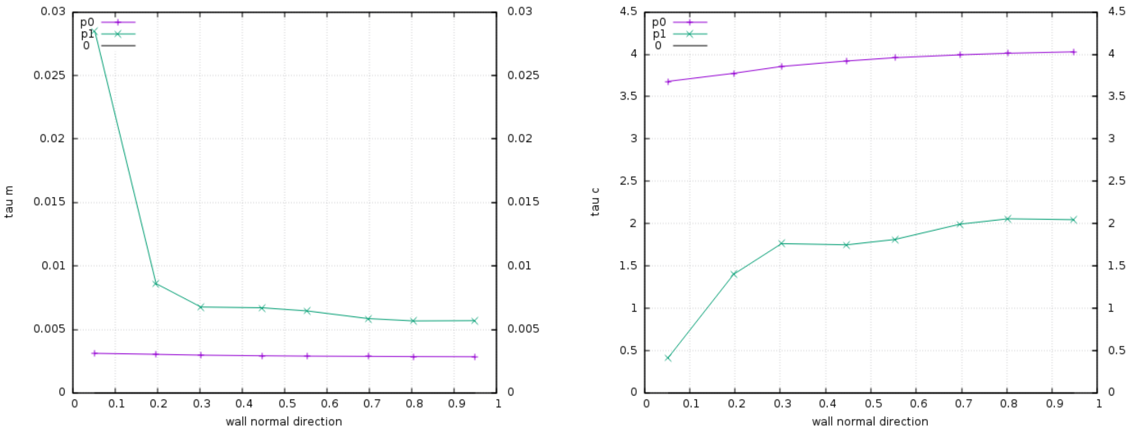

(a) τ_M

(b) τ_C

Figure 7.8: τ_M and τ_C distribution for optimizations. p0, baseline run (purple); p1, optimized run (green)

This section has shown that a level of control can be exerted on the flow profiles by modifying the approximation of the local Green's function. The sensitivity of the formulation to coefficient combinations outside the shown regions often yields unstable results, for which at this point it will be assumed that this is the maximum level of control that can be achieved with this approach. The next section shows an alternative formulation and its effects in an attempt to obtain improved results.

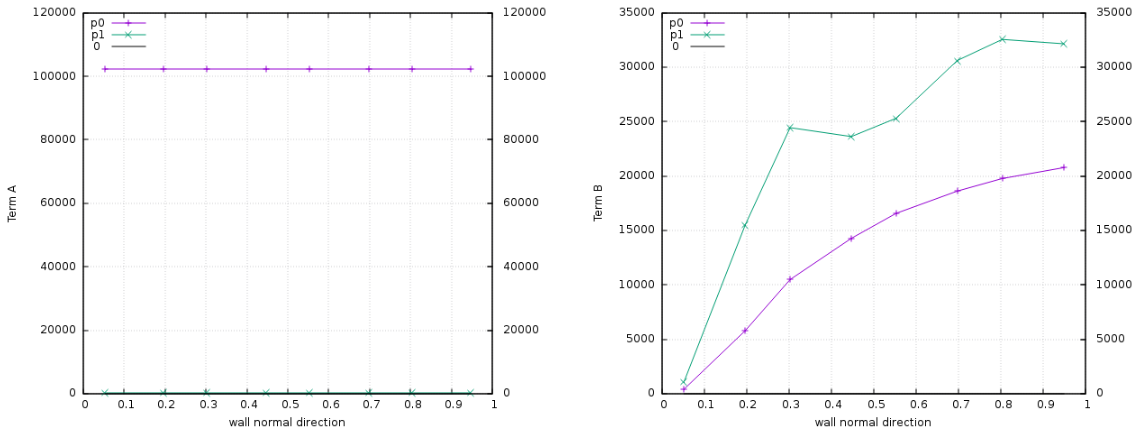

(a) Term A (b) Term B

Figure 7.9: Distribution of the τ_M components in wall normal direction. p0, baseline run (purple); p1, optimized run (green)

7.2 The asymptotic expansion approach

From a test of an asymptotic expansion form to model the small scales for the Burgers equation, as seen in section 4.2; a similar approach was implemented in the context of the NSE in an attempt to improve the results of a LES simulation. Following the previously explained logic, the stabilization term for the small-scales was modified. Starting from (5.22) and expanding, a second term (dependent of the square of the residual of the large scales) is introduced such that:

$$\boldsymbol{u'} = \boldsymbol{u'}_1 + \boldsymbol{u'}_2 = -\boldsymbol{\tau_{Baz}}\boldsymbol{\mathcal{R}} + \eta\varphi\boldsymbol{\mathcal{R}}^2 \tag{7.5}$$

Where η once again represents a dimensional consistency function, $\varphi = \varphi(y)$ is the distribution function, and $\boldsymbol{\mathcal{R}}^2$ is a column vector resulting of a term-wise squaring of $\boldsymbol{\mathcal{R}}$ such that:

$$\boldsymbol{\mathcal{R}}_i^2 = \boldsymbol{\mathcal{R}}_i * \boldsymbol{\mathcal{R}}_i \tag{7.6}$$

Given the form of the curve employed in the distribution function, the definition of $\varphi(y)$ results in:

$$\varphi(y) = \begin{cases} \frac{\gamma_3}{C} y(y-1.0)^{\gamma_4} & 0 \le y < 1 \\ \frac{\gamma_3}{C}(2.0-y)(y-1.0)^{\gamma 4} & 1 \le y \le 2 \end{cases} \tag{7.7}$$

Where C represents a normalization parameter similar to the one described in section 4.2. Figure 7.10 shows an example of the distribution function in wall normal direction for $\gamma_{3,4} = 20$, where once again, the effects of $\boldsymbol{u'}_2$ are concentrated on the boundary layers.

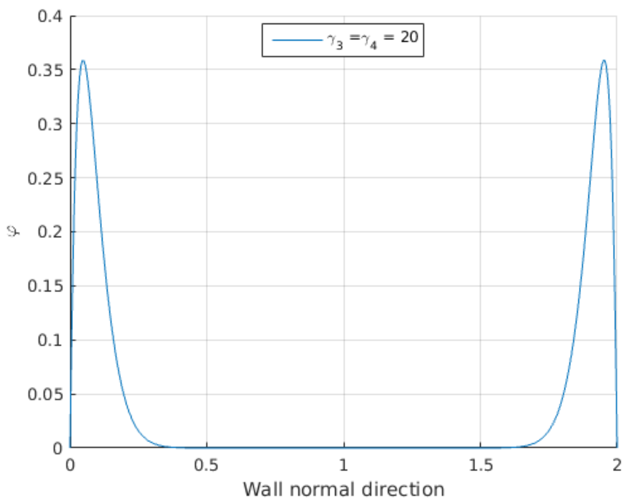

Figure 7.10: Distribution function in wall normal direction for the channel flow case

While the assumed form for the additional term in the asymptotic expansion was sufficient for the Burgers equation, it turned out to be insufficient for this much more complicated NSE cases, where instabilities were encountered for all but the smallest values of γ_3, thus resulting in negligible improvements. A more detailed design procedures for the form of this term, possibly incorporating an energy stability analysis is required. This could not be attempted here due to time constrains.

7.3 Green's function optimization with a distribution function

As observed and explained in subsection 4.2, a large component of the improvements obtained by the asymptotic expansion formulation for the Burgers equation, derived from the use of a distribution function. While such asymptotic expansion proved to be significantly more complex to implement in the context of the NSE, an alternate approach was employed to further improve the results. A distribution function was incorporated to the SGS model such that it becomes:

$$\tau_M = \varphi(y) \left[\gamma_0 \, \frac{1}{\Delta t^2} + \gamma_1 \; \overline{\boldsymbol{u}} \cdot \boldsymbol{G} \overline{\boldsymbol{u}} + \gamma_2 \; \nu^2 \boldsymbol{G} : \boldsymbol{G} \right]^{-1/2} \tag{7.8}$$

Where the distribution function $\varphi(y)$ is given as:

$$\varphi(y) = \begin{cases} 1.0 - \gamma_5(y)(y-1.0)^{\gamma_6} & 0 \leq y < 1 \\ 1.0 + \gamma_5(2.0-y)(y-1.0)^{\gamma_6} & 1 \leq y \leq 2 \end{cases} \tag{7.9}$$

Starting from an initial optimization of (7.1), i.e. $\gamma_0 = 0.01$ and $\gamma_1 = 5.0$, an additional improvement was attempted by localizing the effects of $\boldsymbol{\tau_{Baz}}$ through the use of (7.9). Knowing the location of the integration points in the proximity of the boundary layers, the free parameter γ_6 was fixed for a value of $\gamma_6 = 10$. A single-dimensional optimization run for γ_5 was made, in the range $\gamma_5 = [-40,\ 40]$, for which the distribution function takes the form shown in figure 7.11. To be noticed from here that the "base" value of such function is 1.0, same which maintains an unmodified formulation of $\boldsymbol{\tau_{Baz}}$ in the center channel. The sweep of γ_5 delivers the response curves shown in figure 7.12, which have a minor disagreement in the value of the optimal value of γ_5 and do not show values for $\gamma_5 > 25$ provided that no convergence was achieved for them. It is thus important to point out that this sweep has been made with increments given as $\Delta\gamma_5 = 5$ for which the real optimum value might exist somewhere in between the ones obtained.

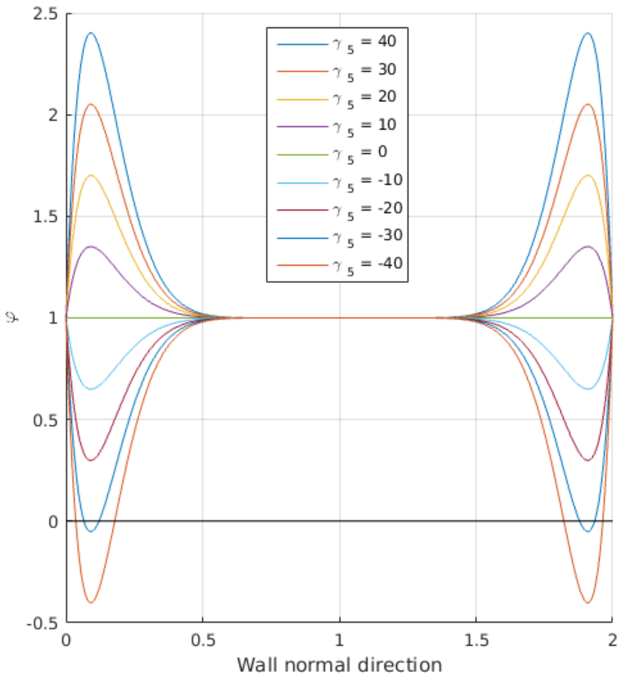

Figure 7.11: Distribution function in wall normal direction for the channel flow case

An LES run with the obtained values of $\gamma_{0,1}\,{}_{,5}$ is now done and its results shown in figure 7.13. Once again, to be seen from here that a further control has been obtained over the profiles. However, the simulation norm is based on the reference values of uBulk and uMean, therefore the fluctuations are not considered in the modifications to the γ_i coefficients. Consequently this results in a consistent improvement for the match of the mean velocities, but only in some cases for the fluctuations profiles, as previously explained, the combination of low grid resolution and low-Re effects originate this behaviors.

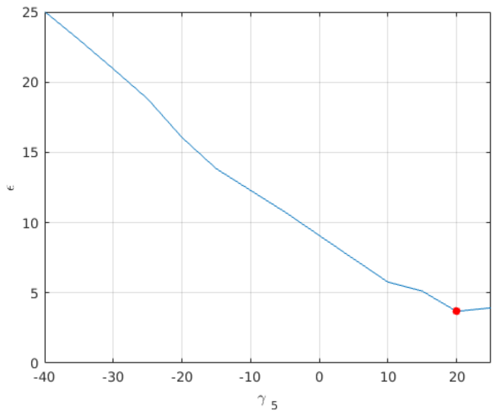

(a) u Bulk

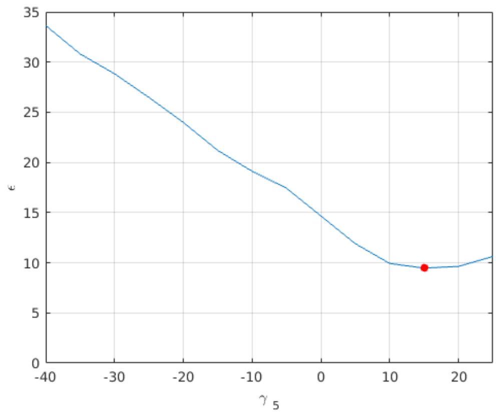

(b) u Mean

Figure 7.12: Response surfaces for optimization runs

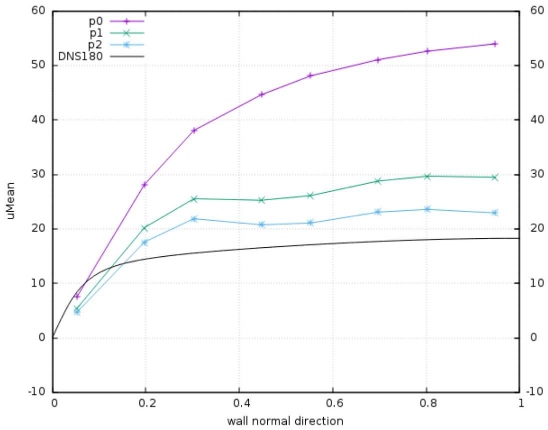

(a) u Mean

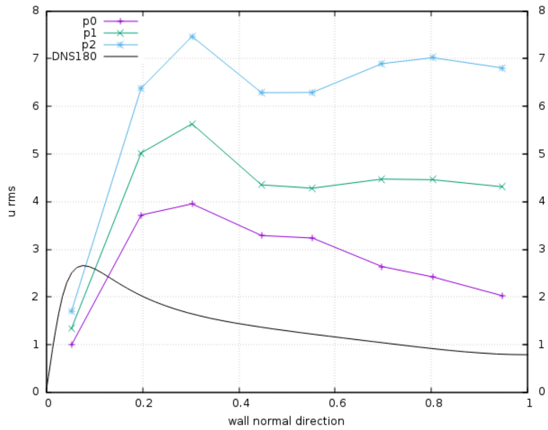

(b) u RMS

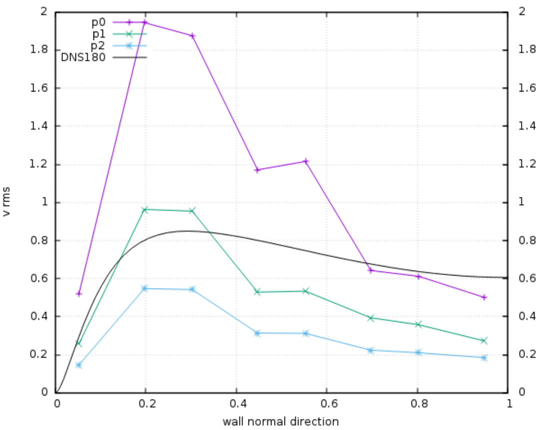

(c) v RMS

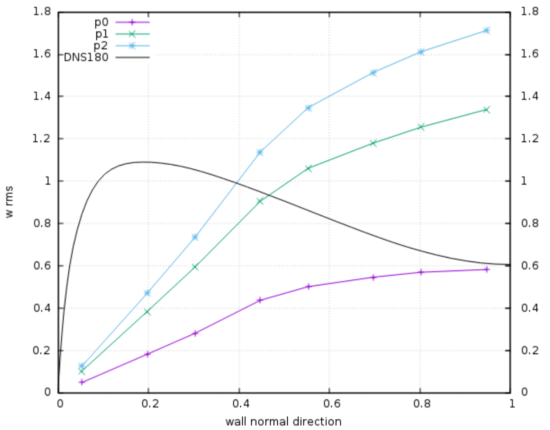

(d) w RMS

Figure 7.13: Statistics profiles for optimization runs. p0, baseline run (purple); p1, $\gamma_{0,1}$ optimized run (green), p2, γ_5 optimized run (blue)

7.4 Spatial refinements and boundary conditions treatment

With this in mind, a test was made for an optimization of $\gamma_{0,1}$ in a 16^3 mesh for $Re_\tau = 180$. The results displayed in figure 7.14, show that in obtaining a closer match of the mean velocities as dictated by the simulation norm, a parallel trend is seen for the fluctuations profiles. Additionally, these runs were performed for a weak imposition of boundary conditions, for which in general, the g-method provided the best results. It is important to point out that these results were subject to more "conservative" coefficients, given that their computation cost is significantly more elevated and thus, their stability region more expensive to determine. However, it is also necessary to say that since a larger part of the solution is now resolved, thus easing the load on the u' approximations, a reduced the authority of the optimizations is now observed given that the influence of u' is smaller.

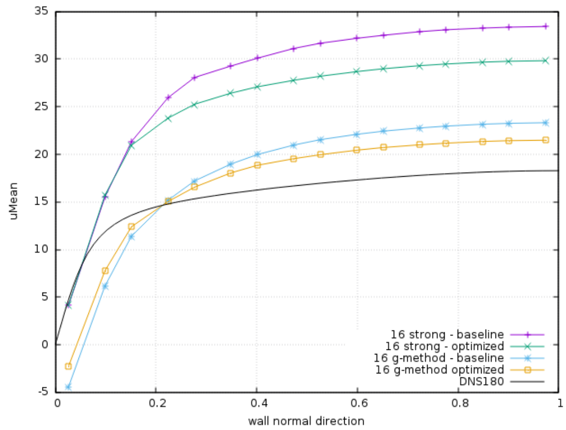

(a) u Mean

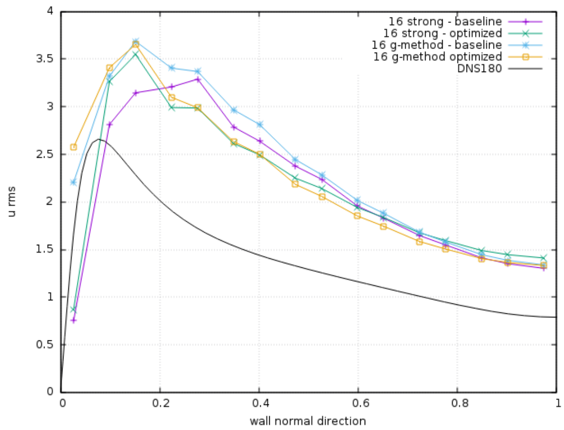

(b) u RMS

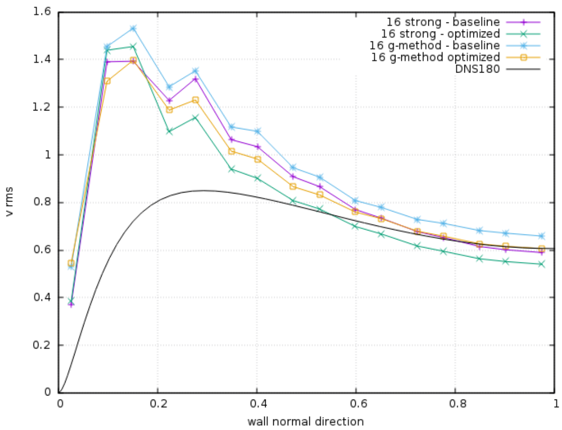

(c) v RMS

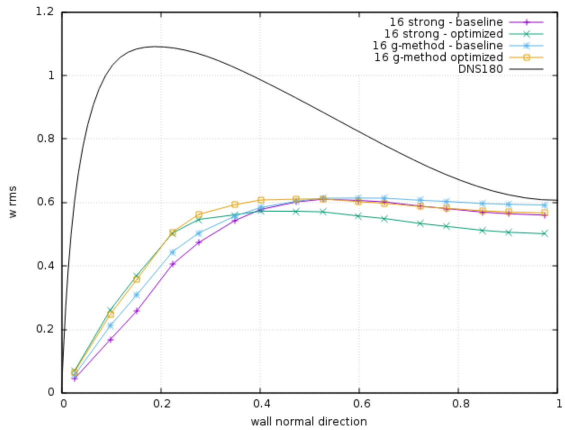

(d) w RMS

Figure 7.14: Statistics profiles for optimization runs in 16^3, $Re_\tau = 180$

This same loss of authority is further evidenced in tests for a 24^3 mesh. As seen in figure 7.15, especially the means profile seems almost insensitive to modifications in the γ_0 parameter. The employed boundary condition enforcement method was the weak imposition, and as discussed in 5.2, a magnitude reduction of the negative wall velocities is appreciated, as the increased grid refinement drives the method to resemble Dirichlet B.Cs.

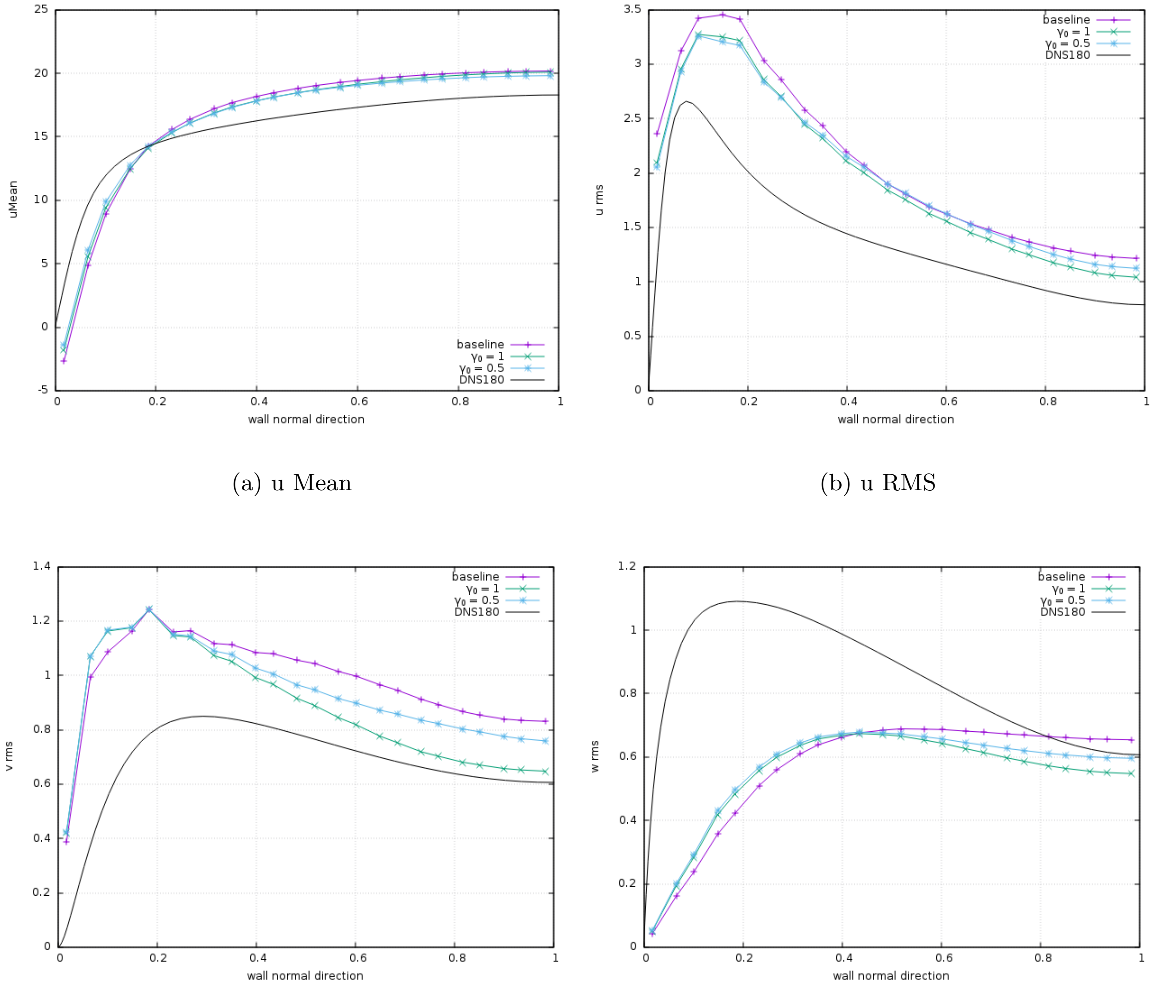

(a) u Mean

(b) u RMS

(c) v RMS

(d) w RMS

Figure 7.15: Statistics profiles for optimization runs in 24^3, $Re_\tau = 180$, g-method

Chapter 8

Conclusions

The use of modified VMM SGS models has been explored with aims to establish the feasibility of employing them as coupling terms for hybrid methods. Through relatively simple modifications to existing formulations, improved results have been obtained for LES simulations while employing statistical data to feed the models. The obtained profiles are indicative of the potential of this method. While this work is intended to set the base knowledge for a more complex methodology, it has demonstrated that a certain level of control can be achieved over the results.

A response surface technique was used for the proposed improvements. While this method is expensive in the context of unsteady three dimensional computations, it was employed with the objective of understanding the solution spaces. Some of the results have demonstrated to loose exactness in the fluctuations profiles while obtaining closes matches in the bulk and mean velocities. This issue might derive from the fact that the optimization solutions spaces are complex. A low resolution exploration of these might be overlooking alternate solutions. The use of the Bazilevs $\boldsymbol{\tau}$ approximation in the NSE case appears to be limiting. Although appropriate in well resolved regions, a formulation with a much higher solution dependence appears to be necessary to improve control authority in coarse regions.

As pointed out by Nicoud et al. (2011), a match of both the mean and fluctuations profiles is essentially no easy task when attempting to reproduce the logarithmic law of the wall with suboptimal controls using a wall stress model. The approach described here is different in that we also consider SGS model adaptations. In the future, this issue is expected to be addressed through the use of "automatic" optimization methods such as Artificial Neural Networks, variational Germano techniques, or Goal-Oriented optimization operating both on the wall boundary condition and in the interior.

Another source of error might lie in the assumption of quasi-static subscales. As demonstrated, this assumption provides a considerable relaxation of the formulations complexity, however this might be introducing a large cost in the sense of the results quality. Work by Codina et al. (2007) has indicated that this is not an assumption of negligible consequences; which seems to be true here, given that the unresolved structures in an 8^3 mesh might be expected to be quite large, and thus an assumption of instantaneous responses to the resolved scales could be bold assumption.

8.1 Recommendations

For future work, some additional considerations are now suggested.

A redefinition of the proposed norms could improve the results if these include the statistical data of the fluctuations. Being the ultimate goal of this research to couple RANS and LES methods, considering information of the Reynolds stresses might provide improved paths to matching the results.

The use of dynamic subscales could also be considered. While this introduces an ODE formulation for the otherwise "simple" small-scales approximations, potentially adding complexity to the interpretation of future results, they might account for a large amount of effects in the overall flow.

The ideas of weak B.Cs. and g method were slightly explored in this framework, however the obtained improvements suggest that further exploration of these methods could provide a better match of the profiles.

In the context of the NSE, the implementation of an asymptotic expansion form for u' yielded what appear to be ineffective results. It is important to point out that the assumptions for this formulation suggested simple forms. In the future, the use of space-time training norms could be used to evaluate alternate candidate forms, which within itself poses another optimization exercise. The energy evolution in the flow can also be tested to ensure the resulting models are stable.

Additionally, the possibility of obtaining an increased control over the fluctuation profiles can be explored through the use of a modified matrix for $\boldsymbol{\tau}$. While recalling that the one employed in this work is a diagonal 4×4 matrix of the from:

$$\boldsymbol{\tau} = \begin{bmatrix} \tau_M & 0 & 0 & 0 \\ 0 & \tau_M & 0 & 0 \\ 0 & 0 & \tau_M & 0 \\ 0 & 0 & 0 & \tau_C \end{bmatrix}$$

an alternate (non-diagonal) form might aid in an attempt to improve the simultaneous matching of the fluctuations profiles while minimizing the simulation norm. Given the explored ideas, this matrix itself can be subject to optimization methods if a series of $\gamma_i \tau_M$ are introduced in its off-diagonal terms.

Bibliography

Ido Akkerman. *Adaptive Variational Multiscale Formulations using the Discrete Germano Approach*. PhD thesis, Delft University of Technology, 2009.

E Albrecht. Residual-based rans/les coupling for the burgers equation, 2013.

Jeffrey S Baggett. On the feasibility of merging les with rans for the near-wall region of attached turbulent flows. *Annual Research Briefs*, pages 267–277, 1998.

Y Bazilevs, VM Calo, JA Cottrell, TJR Hughes, A Reali, and G Scovazzi. Variational multiscale residual-based turbulence modeling for large eddy simulation of incompressible flows. *Computer Methods in Applied Mechanics and Engineering*, 197(1):173–201, 2007a.

Y Bazilevs, C Michler, VM Calo, and TJR Hughes. Weak dirichlet boundary conditions for wall-bounded turbulent flows. *Computer Methods in Applied Mechanics and Engineering*, 196(49):4853–4862, 2007b.

JM Burgers. On the coalescence of wavelike solutions of a simple non-linear partial differential equation. *Proc. KNAW B, LVII*, 1:45–72, 1954.

Johannes Martinus Burgers. A mathematical model illustrating the theory of turbulence. *Adv. in Appl. Mech.*, 1:171–199, 1948.

L Chen, WN Edeling, and SJ Hulshoff. Pod enriched boundary models and their optimal stabilisation. *International Journal for Numerical Methods in Fluids*, 77(2):92–107, 2015.

Ramon Codina, Javier Principe, Oriol Guasch, and Santiago Badia. Time dependent subscales in the stabilized finite element approximation of incompressible flow problems. *Computer Methods in Applied Mechanics and Engineering*, 196(21):2413–2430, 2007.

Juan C del Álamo and Javier Jiménez. Spectra of the very large anisotropic scales in turbulent channels. *Physics of Fluids*, 15(6):L41, 2003.

Thijs Durieux. Exploring the use of artificial neural network based subgrid scale models in a variational multiscale formulation, 2015.

Wouter N Edeling. Improved representations of unresolved scales using optimization techniques, 2011.

Leopoldo P Franca and Sérgio L Frey. Stabilized finite element methods: Ii. the incompressible navier-stokes equations. *Computer Methods in Applied Mechanics and Engineering*, 99(2): 209–233, 1992.

Jochen Froehlich and Dominic von Terzi. Hybrid les/rans methods for the simulation of turbulent flows. *Progress in Aerospace Sciences*, 44(5):349–377, 2008.

F Hamba. An approach to hybrid rans/les calculation of channel flows. *Engineering turbulence modelling and experiments*, 5:297–306, 2002.

Sergio Hoyas and Javier Jiménez. Reynolds number effects on the reynolds-stress budgets in turbulent channels. *Physics of Fluids (1994-present)*, 20(10):101511, 2008.

Thomas JR Hughes. Multiscale phenomena: Green's functions, the dirichlet-to-neumann formulation, subgrid scale models, bubbles and the origins of stabilized methods. *Computer methods in applied mechanics and engineering*, 127(1):387–401, 1995.

Thomas JR Hughes and Michel Mallet. A new finite element formulation for computational fluid dynamics: Iii. the generalized streamline operator for multidimensional advective-diffusive systems. *Computer Methods in Applied Mechanics and Engineering*, 58(3):305–328, 1986.

Thomas JR Hughes, LP Franca, and M Mallet. A new finite element formulation for computational fluid dynamics: I. symmetric forms of the compressible euler and navier-stokes equations and the second law of thermodynamics. *Computer Methods in Applied Mechanics and Engineering*, 54(2):223–234, 1986.

Thomas JR Hughes, Luca Mazzei, and Kenneth E Jansen. Large eddy simulation and the variational multiscale method. *Computing and Visualization in Science*, 3(1-2):47–59, 2000.

Thomas JR Hughes, Guglielmo Scovazzi, and Leopoldo P Franca. *Multiscale and stabilized methods*. Wiley Online Library, 2004.

SJ Hulshoff, EA Munts, and J Labrujere. Wall-stress boundary conditions for variational-multiscale les. *International Journal for Numerical Methods in Fluids*, 66(11):1341–1353, 2011.

John Kim, Parviz Moin, and Robert Moser. Turbulence statistics in fully developed channel flow at low reynolds number. *Journal of fluid mechanics*, 177:133–166, 1987.

J Larsson, FS Lien, and E Yee. The artificial buffer layer and the effects of forcing in hybrid les/rans. *International Journal of Heat and Fluid Flow*, 28(6):1443–1459, 2007.

Florian R Menter, Jochen Schütze, and Mikhail Gritskevich. Global vs. zonal approaches in hybrid rans-les turbulence modelling. In *Progress in Hybrid RANS-LES Modelling*, pages 15–28. Springer, 2012.

FR Menter and Y Egorov. The scale-adaptive simulation method for unsteady turbulent flow predictions. part 1: theory and model description. *Flow, Turbulence and Combustion*, 85 (1):113–138, 2010.

Robert D Moser, John Kim, and Nagi N Mansour. Direct numerical simulation of turbulent channel flow up to re= 590. *Phys. Fluids*, 11(4):943–945, 1999.

Franck Nicoud, Hubert Baya Toda, Olivier Cabrit, Sanjeeb Bose, and Jungil Lee. Using singular values to build a subgrid-scale model for large eddy simulations. *Physics of Fluids (1994-present)*, 23(8):085106, 2011.

FT Nieuwstadt and JA Steketee. *Selected papers of JM Burgers*. Springer Science & Business Media, 2012.

NV Nikitin, Franck Nicoud, B Wasistho, KD Squires, and PR Spalart. An approach to wall modeling in large-eddy simulations. *Physics of Fluids (1994-present)*, 12(7):1629–1632, 2000.

Ugo Piomelli, Elias Balaras, Kyle D Squires, and Philippe R Spalart. Zonal approaches to wall-layer models for large-eddy simulations. *AIAA Paper*, 3083, 2002.

Ugo Piomelli, Elias Balaras, Hugo Pasinato, Kyle D Squires, and Philippe R Spalart. The inner–outer layer interface in large-eddy simulations with wall-layer models. *International Journal of heat and fluid flow*, 24(4):538–550, 2003.

Stephen B Pope. *Turbulent flows*. Cambridge university press, 2000.

Patrick J Roache. Code verification by the method of manufactured solutions. *Journal of Fluids Engineering*, 124(1):4–10, 2002.

Christopher J Roy. Review of code and solution verification procedures for computational simulation. *Journal of Computational Physics*, 205(1):131–156, 2005.

Guglielmo Scovazzi. *Multiscale methods in science and engineering*. PhD thesis, Stanford University, 2004.

Farzin Shakib and Thomas JR Hughes. A new finite element formulation for computational fluid dynamics: Ix. fourier analysis of space-time galerkin/least-squares algorithms. *Computer Methods in Applied Mechanics and Engineering*, 87(1):35–58, 1991.

Farzin Shakib, Thomas JR Hughes, and Zdeněk Johan. A new finite element formulation for computational fluid dynamics: X. the compressible euler and navier-stokes equations. *Computer Methods in Applied Mechanics and Engineering*, 89(1):141–219, 1991.

PR Spalart, WH Jou, M Strelets, and SR Allmaras. Comments on the feasibility of les for wings, and on a hybrid rans/les approach. *Advances in DNS/LES*, 1:4–8, 1997.

Trond Steihaug. The conjugate gradient method and trust regions in large scale optimization. *SIAM Journal on Numerical Analysis*, 20(3):626–637, 1983.

Heng Xiao and Patrick Jenny. A consistent dual-mesh framework for hybrid les/rans modeling. *Journal of Computational Physics*, 231(4):1848–1865, 2012.